Journal of Composite Materials
52(30):4151–4188

DOI: 10.1177/0021998318776721
www.sagepub.com/
SAGE

Damage initiation and evolution during monotonic cooling of laminated composites

Ever J. Barbero[1] and Javier Cabrera Barbero[2]

Abstract

The objective of this work is to develop a methodology to predict matrix damage initiation and evolution in laminated composites subjected to monotonic cooling using discrete damage mechanics and a careful characterization of the required temperature-dependent material properties. Since prediction of thermo-mechanical damage requires precise knowledge of the temperature-dependent properties of the material, back-calculation of fiber and matrix properties from different sources is included. The proposed methodology is flexible in that it can be adapted to the availability of experimental data. A compilation of literature data is developed to estimate the properties of several fiber and matrix systems. Prediction of lamina and laminate temperature-dependent properties are compared with available data. Furthermore, temperature-dependent fracture toughness of four material systems are estimated from available crack density data. For the material systems studied, it is found that temperature-independent fracture toughness is satisfactory for prediction of damage initiation, evolution, and saturation.

Keywords

Damage; coefficient of thermal expansion; thermomechanical; temperature dependent; cryogenic; energy release rate; fracture; micromechanics; elastic properties

¡[1]Professor, West Virginia University, Morgantown, WV 26506-6106
[2]Graduate Research Assistant, West Virginia University, Morgantown, WV 26506-6106

Corresponding author:
Ever J. Barbero, 711 ESB, West Virginia University, Morgantown, WV 26506-6106

Prepared using sagej.cls *[Version: 2016/06/24 v1.10]*

Introduction

A broad variety of composite structures, such as aircraft, satellites, thermoelectric generators, cryogenic storage, and so on, are subjected to thermally induced stress and strain that may result in damage and eventual failure. Due to accumulation of damage, these structures may loose their ability to sustain loads, or to transfer stress between their constituents, diminishing their efficiency, or loosing their hermeticity, or compromising their ability to contain liquids and gases, etc. Matrix cracking also jeopardizes the integrity of the reinforcements since cracks provide access to corrosive environmental attack. Therefore, the objective of this work is to predict damage initiation and evolution up to crack saturation in laminated composites subjected to monotonic cooling.

Due to difference in coefficient of thermal expansion (CTE) among laminas with different orientations, thermal stress and strain are induced, which often cause transverse matrix cracking of the laminas. Prediction of thermo-mechanical damage requires precise knowledge of the temperature-dependent properties of the material, including elastic and fracture properties. Temperature ranges of interest include Low Earth Orbit (LEO [-100 to 66 C])[1], Geostationary Earth Orbit (GEO [-156 to 121])[2–8], and cryogenic tanks (Liquid Nitrogen, Oxygen, Helium, CO_2, Hydrogen, etc.). Waste Heat Recovery devices [24 to 200 C] are also susceptible to matrix cracking when cooling down from their operating temperature[9,10].

The material properties of polymer matrix composites change with temperature, mainly due to the temperature-dependent properties of the polymer. Measurement of strength and thermal expansion of laminated composites as a function of temperature is reported for example in[11–16]. Temperature dependence of lamina properties are reported for example in[17–22].

Since temperature-dependent data for most material systems is scarce, micromechanics is often used to predict lamina data from fiber and matrix data. Temperature-dependent properties for fiber and matrix are also difficult to find, but once lamina data for a few material system are found, the fiber and matrix properties can be back calculated, then used to predict lamina properties for other combinations of fiber/matrix at similar, yet different, values of fiber volume fraction. Although many micromechanics models exist, most have been derived for isotropic fibers, although carbon fibers are transversely isotropic.

The lamina properties that are most sensitive to temperature are the matrix dominated properties, namely $E_2(T), G_{12}(T)$, and $\alpha_2(T)$. Prediction of these properties are affected by the transverse properties of the fiber E_T, G_T, α_T as well as those of the polymer. Therefore, it is important to use a micromechanics model that accounts for transverse isotropy of the fiber. Furthermore, it is advantageous to use a micromechanics model that can predict all five properties of the transversely isotropic lamina using a unified formulation and that yields accurate predictions without requiring adjustable parameters such as stress partitioning[23], etc. The periodic microstructure model (PMM) satisfies all of the aforementioned requirements and it has been extensively validated for

elastic and creep/relaxation behavior of unidirectional composites[24–26]. PMM is described in App. 2 of[23] and implemented in[27].

For isotropic fibers, the transverse CTE of the lamina can be estimated by the rule of mixtures[23,28]. Strife and Prewo[29] proposed a modification to account for transversely isotropic properties of the fiber. Their modification is not derived from mechanics or physical principles but just a substitution of ν_A, α_T for ν_f, α_f in the rule of mixtures formula[28]. Predictions using either[28] or[29] are somewhat accurate for some materials such as Kevlar/Epoxy but no so for other materials[29]. The model proposed by Levin[30,31] (see eq. (9) in Section "Coefficients of Thermal Expansion") is intrinsically exact and able to calculate the three CTE values for an orthotropic lamina, but relies on the estimated elasticity tensor for the lamina. Therefore, the accuracy of Levin's method is only limited by the accuracy of the estimate for the elasticity tensor. Levin's work was extended in[32] for three-phase composites and used in an extensive study of thermal properties of composite materials in[3,33].

The matrix is always assumed to be isotropic with elastic properties $E_m(T), \nu_m(T)$, and $\alpha_m(T)$, were T is the temperature. On the other hand, the fibers are assumed to be transversely isotropic with properties $E_A, E_T, G_A, \nu_A, \nu_T, \alpha_A, \alpha_T$. Carbon fibers are reported to be almost temperature independent[2–8] in the temperature ranges for LEO [-100–66] C and GEO [-156–121] C.

Poisson's ratio ν_m of polymers is influenced by the free volume available in the material. At high temperatures, the polymer chains become rubbery and the Van der Waals forces, which control the inter-chain bonds, are weaker leading to higher Poisson's ratio. Conversely, at low temperatures, the polymer becomes brittle with lower Poisson's ratio. Some authors report Poisson's ratio almost constant with temperature for composite laminas with epoxy resins[34,35]. Others bracket the Poisson ratio's of polymer at low temperatures between 0.29 and 0.39[36].

Below the glass transition temperature T_g, the molecular structure of polymers transitions from a rubbery to glassy state, and becomes more and more rigid and brittle at lower temperatures. The elastic modulus E_m increases markedly and the strain to failure ϵ_{mu} decreases[37–40] at colder temperatures, culminating at cryogenic liquid nitrogen (LN_2) temperature (-196 C)[41], which is the lowest limit considered in this work.

Carbon-fiber composite data has been used to demonstrate the applicability of the proposed methodology. The material systems used in this study are: Cytec P75/934, Amoco P75/1962, Narmco T300/5208, and Hexcel AS4/3501-6. Some material property data that are necessary for thermo-mechanical analysis are unavailable in the literature and the type of data missing is not the same for every material system. For example, the transverse CTE of AS4 and T300 fibers are not available. The temperature range of lamina and matrix data varies drastically among different sources. Sometimes there is a single data point available at low temperature using liquid Helium (-231 C)[39,42] or the range of temperature is too narrow[37,38,43]. Some experimental data show no higher

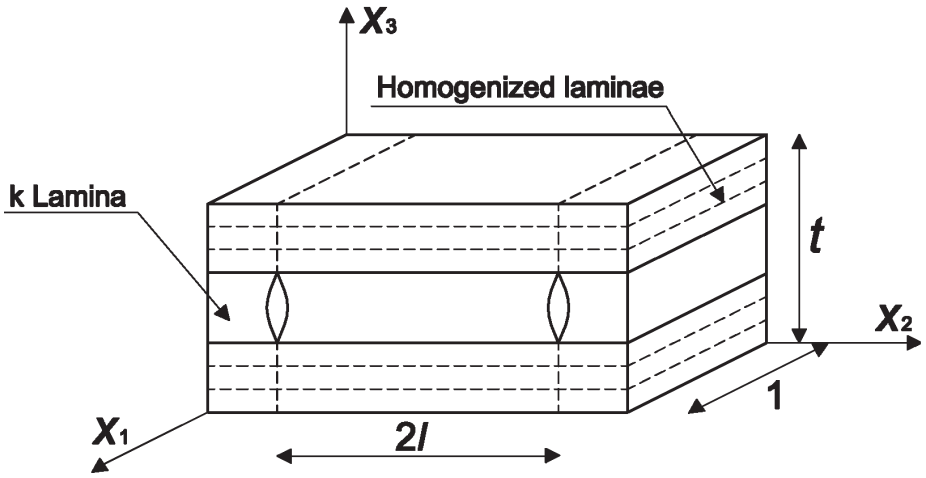

Figure 1. Representative volume element for Discrete Damage Mechanics (DDM).

rigidity at cryogenic temperature[44], or even softening[45]. No definite conclusion is available in the literature about rigidity below −200 C.

Since availability of material properties *are different* for each fiber, matrix, and material system (lamina), the proposed methodology must be flexible to adapt to the availability of data. Consequently, a generic outline of the proposed methodology is presented first in Sections "Constituent Properties," "Coefficients of Thermal Expansion," and "Critical Energy Release Rates," followed by detailed, self-contained descriptions of the complete process for each fiber, matrix, and composite material system (lamina). In an effort to have complete descriptions of the parameter estimation process for each material, some repetition of calculation steps is unavoidable.

Discrete Damage Mechanics

The bibliography on distributed damage in composite laminates is extensive[46,47]. Among the multitude of damage models available, discrete damage mechanics (DDM)[48] is attractive for this study because, in addition to the usual elastic properties, it requires only two values of critical energy release rate (critical ERR), G_{Ic} and G_{IIc}, to predict both damage initiation and evolution due to transverse and in-plane shear stresses for general laminates subjected to general loads[49]. DDM is an objective (mesh independent) constitutive model, meaning that when implemented in FEM software, it does not require guessing of characteristic length L_c in order to reduce mesh dependency. Furthermore, DDM is available as a plugin for Abaqus[50] and ANSYS[51], and it has been extensively validated.

DDM is based on an analytical solution[48] of the displacement field inside a representative volume element (RVE, Fig. 1) encompassing the laminate

thickness t with N laminas, a unit length along the fiber direction of the cracking lamina $k = c$, and a distance $2\ell = 1/\lambda_c$. Homogenization of the damaged stiffness of the N laminas, coupled with an iterative procedure allows all laminas $k = 1 \dots N$ in a laminate to be cracking simultaneously with different crack density λ_k values at a given time. For a given damage state $\lambda = \{\lambda_k\}^T$ and applied 2D strain field $\epsilon = \{\epsilon_1, \epsilon_2, \gamma_6\}^T$ at a Gauss integration point of a shell element, DDM determines the local 3D displacement field $u_i(x_j)$ analytically, with $i, j = 1 \dots 3$, from which it calculates the local strain field and stress field including intralaminar stresses, as well as damaged lamina $[Q]$, damaged laminate stiffness matrices, and energy release rates (ERR) in modes I and II, G_I, G_{II}. The later are used in an interacting damage initiation and evolution criterion

$$g = (1-r)\sqrt{\frac{G_I(\lambda,\epsilon)}{G_{Ic}}} + r\frac{G_I(\lambda,\epsilon)}{G_{Ic}} + \frac{G_{II}(\lambda,\epsilon)}{G_{IIc}} - 1 \leq 0 \tag{1}$$

with $r = G_{Ic}/G_{IIc}$. Note that critical ERR G_{Ic}, G_{IIc} are the only material properties needed to predict both initiation and evolution of crack density. No hardening exponents or any other damage evolution material properties are needed to describe the kinetic evolution of damage. The ERR values G_I, G_{II} in modes $i = I, II$ are calculated as

$$G_i = \frac{U_{i,a} - U_{i,b}}{\Delta A_c} \tag{2}$$

where $U_{I,a}, U_{I,b}, U_{II,a}, U_{II,b}$ are the elastic strain energies in modes I and II, for crack densities λ_a and $\lambda_b = 2\lambda_a$, and ΔA is the increment of crack area when a new crack propagates (Sect. 8.4.7 in [23]). Mode decomposition is achieved by splitting the strain energy U into mode I (opening) and II (shear) and adding the contribution of each lamina $k = 1 \dots n$ as follows

$$U_I = \frac{V_{RVE}}{2h}\sum_{k=1}^{n} t_k(\epsilon_2 - \widetilde{\alpha}_2^{(k)}\Delta T)\, Q_{2j}^{(k)}(\epsilon_j - \widetilde{\alpha}_j^{(k)}\Delta T) \tag{3}$$

$$U_{II} = \frac{V_{RVE}}{2h}\sum_{k=1}^{n} t_k(\epsilon_6 - \widetilde{\alpha}_6^{(k)}\Delta T) Q_{6j}^{(k)}(\epsilon_j - \widetilde{\alpha}_j^{(k)}\Delta T) \tag{4}$$

where $h = \sum_{k=1}^{n} t_k$, $\epsilon_6 = \gamma_{12}$, and $\widetilde{\alpha}^{(k)}$ are the undamaged CTE of lamina k. Equation (3) is cast in the coordinate system of the cracking lamina k so that ϵ_2 is mode I (crack opening) and ϵ_6 is mode II (crack shear). Laminate ultimate failure is predicted by a fiber damage and failure criterion [52].

DDM assumes local uniformity of crack spacing and linear distribution of intralaminar stresses. Despite these restrictions, predicted results correlate extremely well with available data for a broad variety of material systems (Carbon and Glass reinforced composites) [53,54], laminate stacking sequences (LSS) [49,55–61] and loading conditions including open hole tension data up to failure [52,62–64].

Table 1. Carbon fiber properties.

Property	AS4	T300	P75
E_A [GPa]	231.000	231.000	517.000
E_T [GPa]	23.453	26.864	11.158
G_A [GPa]	15.764	81.662	10.636
ν_A	0.253	0.156	0.269
ν_T	0.371	0.287	0.306
α_A [10^{-6}/ C]	-0.630	-0.600	-1.46
α_T [10^{-6}/ C]	5.997	11.086	12.500

Since the size of the RVE ($1 \times t \times 1/\lambda_k$) is dictated by the crack density λ_k, not by the element size, and the solution is in terms of displacements, not stress or strain, the predictions of the DDM constitutive model are mesh-density and element-type independent. The only effect of mesh density is on the quality of the stress/strain field. This is a remarkable advantage with respect to cohesive zone constitutive models, which produce results that are mesh-density and element-type dependent, as shown in [53,65,66].

Constituent Properties

The methodology used to calculate the properties of the constituents (fiber and matrix) is presented in this section. If not available in the literature, the elastic properties of the constituents (fiber and matrix) are, in this work, back calculated using periodic microstructure micromechanics (PMM, App. 2 in [23]).

Properties of carbon fibers used in this work are shown in Table 1. The longitudinal modulus E_A and CTE α_A are collected from manufacturer data sheets[67–69]. The rest of fiber properties (E_T, G_A, ν_A, ν_T) and transverse fiber CTE α_T are back calculated as explained in this section and Section "Coefficients of Thermal Expansion", respectively.

Temperature-dependent properties of Epoxy are shown in Tables 2, 3, 4, and 5, back calculated from unidirectional lamina data, as explained in this section and Section "Coefficients of Thermal Expansion". In all cases, the matrix properties (E_m, ν_m, α_m) are represented by a quadratic polynomial

$$P(T) = P_a + P_b\, T + P_c\, T^2 \tag{5}$$

where P is the property, T is the temperature, and P_a, P_b, P_c are the coefficients. In order to get reliable values, experimental data at low, room, and high temperatures are necessary. The back calculation method provides the property $P(T)$ at various temperatures so that the predicted lamina properties fit available experimental data as explained in this section and Section "Coefficients of Thermal Expansion". Then, property values at various temperatures are subsequently fitted with (5). Quadratic polynomial were used also by [3,13,19,33,70–72].

Fiber properties (E_T, G_A, ν_A, ν_T) and matrix properties (E_m, ν_m) (5) are adjusted so that the lamina properties ($E_1, E_2, G_{12}, \nu_{12}, \nu_{23}$) predicted using

Table 2. Quadratic temperature-dependent properties of Epoxy 3501-6 in the range $[180, -200]^o$ C.

Property	P_a	P_b	P_c
E_m [MPa]	4580.4836	-10.6103	0
ν_m	0.3812	$3.8564\ 10^{-5}$	0
α_m $[10^{-6}/\ C]$	38.3445	0.1224	0

Table 3. Quadratic temperature-dependent properties of Epoxy 934 in the range $[-156, 120]^oC$.

Property	P_a	P_b	P_c
E_m [MPa]	5032.7732	-16.7561	0.0251
ν_m	0.3659	$-1.1108\ 10^{-4}$	$-8.6080\ 10^{-7}$
α_m $[10^{-6}/\ C]$	38.7655	0.1524	$-1.32553\ 10^{-4}$

Table 4. Quadratic temperature-dependent properties of Epoxy ERL 1962 in the range $[-156, 120]^oC$.

Property	P_a	P_b	P_c
E_m [MPa]	5032.7732	-16.7561	0.0251
ν_m	0.3659	$-1.1108\ 10^{-4}$	$-8.6080\ 10^{-7}$
α_m $[10^{-6}/\ C]$	49.3143	0.1594	$-4.5090\ 10^{-4}$

Table 5. Quadratic temperature-dependent properties of Epoxy 5208 in the range $[-156, 120]^oC$.

Property	P_a	P_b	P_c
E_m [MPa]	4828.7124	-5.4846	$-5.2164\ 10^{-3}$
ν_m	0.4072	$-3.3332\ 10^{-4}$	$7.9119\ 10^{-7}$
α_m $[10^{-6}/\ C]$	36.6598	0.1887	$-9.5441\ 10^{-5}$

PMM fit available experimental lamina data $(E_1^d, E_2^d, G_{12}^d, \nu_{12}^d)$ available in the literature. The properties are adjusted at each temperature by minimizing the error D calculated as follows

$$D = \frac{1}{N}\sqrt{\sum^{N}\left[\left(\frac{E_1 - E_1^d}{E_1^d}\right)^2 + \left(\frac{E_2 - E_2^d}{E_2^d}\right)^2 + \left(\frac{G_{12} - G_{12}^d}{G_{12}^d}\right)^2 + \left(\frac{\nu_{12} - \nu_{12}^d}{\nu_{12}^d}\right)^2\right]} \tag{6}$$

where N is the number of lamina data points at a given temperature, and superscript d means data. In order to give the same weight to all properties, each term is normalized as shown. Elastic properties from literature or manufacturer data sheet, if available, are used as initial guess for the minimization algorithm.

Denoting by x the value of any of the material properties of interest, and by D the error (6), the value of property x is found when the error D is less than the function tolerance (i.e., error tolerance)[73] $tol^{fun} = 10^{-8}$ and the change in property Δx is less than the step size tolerance $tol^x = 10^{-8}$.

Not all material systems can be characterized exactly with the procedure described above. Variations in the procedure are necessary to make use of the

available data, which varies from material to material. In the following, four matrices and four fibers are characterized, illustrating how to adapt the proposed procedure to make best use of the available data.

Epoxy 3501-6

A large amount of experimental elastic data $(E_1^d, E_2^d, G_{12}^d, \nu_{12}^d)$ exists at room temperature (RT) and high temperature (HT) for AS4/3501-6 unidirectional lamina[4,14,15,17,22,74–76] but at low temperature, only longitudinal modulus data E_1^d at -54 C is available[77]. No matrix-dominated $(E_2^d, G_{12}^d, \nu_{12}^d)$ could be found at low temperature. Back calculation of $E_m(-54C)$ and $\nu_m(-54C)$ from $E_1^d(-54C)$ is not possible because E_1 is a fiber dominated property but E_m, ν_m are matrix dominated properties. Therefore, the temperature-dependent properties E_m, ν_m for Epoxy 3501-6 were adjusted based on available neat resin data[78,79]. In this way, matrix coefficients (5) for E_m, G_m of Epoxy 3501-6 are obtained by interpolation in the range [150,24 C] of the data available in[78,79]. Linear interpolation is sufficiently accurate in this case. The Poisson's ratio ν_m is calculated in terms of E_m, G_m using the isotropic relationship $\nu_m = E_m/(2G_m - 1)$. In this paper, temperature ranges are given from hot to cold because that is the way cooling takes place.

Calculated values of Poisson's ratio ν_m turn out to be virtually constant with temperature. Since the temperature-dependent properties are linearly fitted, based on neat resin data, and they vary smoothly with temperature, they are extrapolated to the whole temperature range of study [180,-200 C] as shown in Figure 2. For predictions, the temperature range in this paper starts at 180 C because that is the most common glass transition temperature of the materials studied. The coldest temperature is -200 C for illustrative purposes only.

Epoxy 934

Elastic properties E_m, ν_m of Epoxy 934 at high (121 C) and room temperature (RT) are taken from the experimental neat resin data in[80]. Then, the elastic properties E_m, ν_m at low temperature (−156 C) of Epoxy 934 are obtained by minimizing the error (6) between T300/934 lamina data $(E_1^d, E_2^d, G_{12}^d, \nu_{12}^d)$ available in[20] and predicted lamina properties $(E_1, E_2, G_{12}, \nu_{12}, \nu_{23})$ calculated using PMM micromechanics. The methodology used is illustrated in Figure 3 by a flowchart. The tolerance[73] used is $tol^x = tol^{fun} = 10^{-8}$.

T300 fiber properties used as input data in PPM are taken from Table 1. Once the elastic properties at room, high, and low temperature have been obtained, the coefficients (5) are calculated by a quadratic interpolation in the range [121,−156 C] and reported in Table 3. The values found for these coefficients are very close to the values reported in[3]. The resulting plot is shown in Figure 4. Unlike Figure 2, the curves in Figure 4 are not linear and thus extrapolation outside of the range of the experimental data may yield exaggerated values. Therefore, for calculation of crack density outside the temperature range of the experimental data from which the temperature dependence is found, the

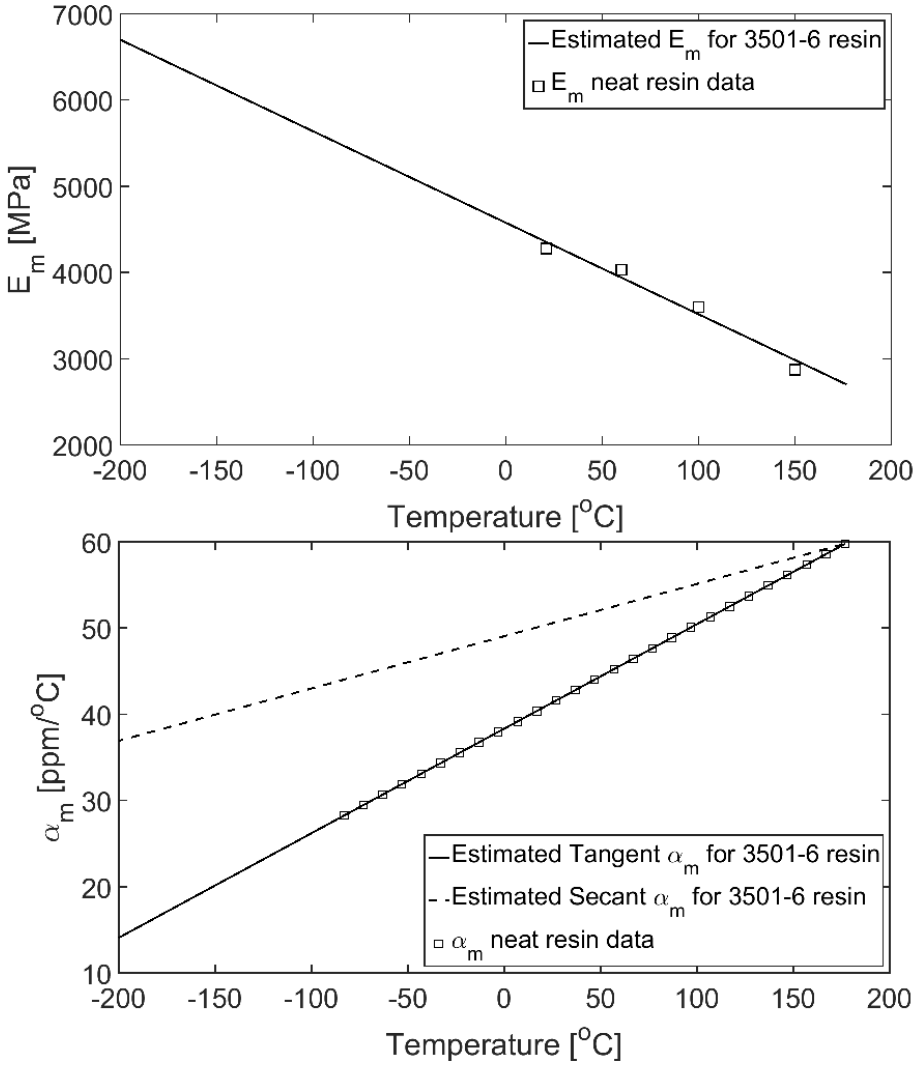

Figure 2. Estimated temperature-dependent modulus E_m (top) and CTE (bottom) for Epoxy 3501-6 extrapolated to the whole temperature range of study [180,-200 C].

matrix properties are assumed to be constant and equal to the end values of the experimental data, as shown in Figure 4.

Epoxy ERL 1962

Epoxy ERL 1962 is similar to Epoxy 934 with added rubbery particles to increase fracture toughness. Lamina data from the literature[21,81–83] for composites using these two resins (934 and ERL 1962) and the same type of fiber have almost identical properties. Only a slightly lower modulus for ERL

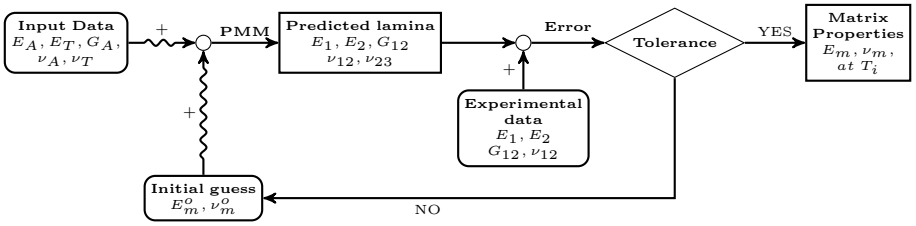

Figure 3. Back calculation method to obtain the temperature-dependent matrix properties at any temperature T_i.

1962 than Epoxy 934 was reported in[81]. Lacking experimental data revealing temperature-dependent properties for neat resin or unidirectional laminas using ERL 1962 matrix, the temperature-dependent *elastic* properties of Epoxy ERL 1962 are assumed in this study to be equal to those of Epoxy 934, but temperature-dependent CTEs are still adjusted to experimental data as shown in Section "Material system: P75/1962".

Epoxy 5208

Elastic properties E_m, ν_m, of Epoxy 5208 are back calculated from lamina elastic data in[11,12] at cryogenic, room, and high temperatures ($-156, 24$, and 121 C). The Poisson's ratio reported in[12] is so high that leads to $\nu_m > 0.5$ for temperatures below -100 C. Such values are incoherent for isotropic polymers at low temperature[35,36]. For this reason, the lamina Poisson's ratio $\nu_{12}^d = 0.24$ at RT was taken from[13] and assumed equal to 0.3 at cryogenic temperature (-156 C), which are typical values for brittle epoxy polymers at very low temperatures[36].

Once the experimental data are collected, the elastic properties E_m, ν_m of Epoxy 5208 at each temperature (-156, 24, and 121 C) are back calculated by minimizing the error (6) between experimental lamina data $(E_1^d, E_2^d, G_{12}^d, \nu_{12}^d)$ available in[12,13,70] and predicted lamina properties $(E_1, E_2, G_{12}, \nu_{12}, \nu_{23})$ using PMM micromechanics. The procedure is illustrated in Figure 3 by a flowchart, with tolerance[73] tol^x and $tol^{fun} = 10^{-8}$. The T300 fiber properties used as input data in PMM are taken from Table 1. Finally, the matrix coefficients (5) of Epoxy 5208 are obtained by a quadratic interpolation of the values obtained at $-156, 24$, and 121 C, then reported in Table 5 and depicted in Figure 5. Similarly to Figure 4, the curves in Figure 5 are nonlinear. Therefore, outside the range of the experimental data from which the temperature dependence is found, the matrix properties are assumed to be constant and equal to the end values of the experimental data, as shown in Figure 5.

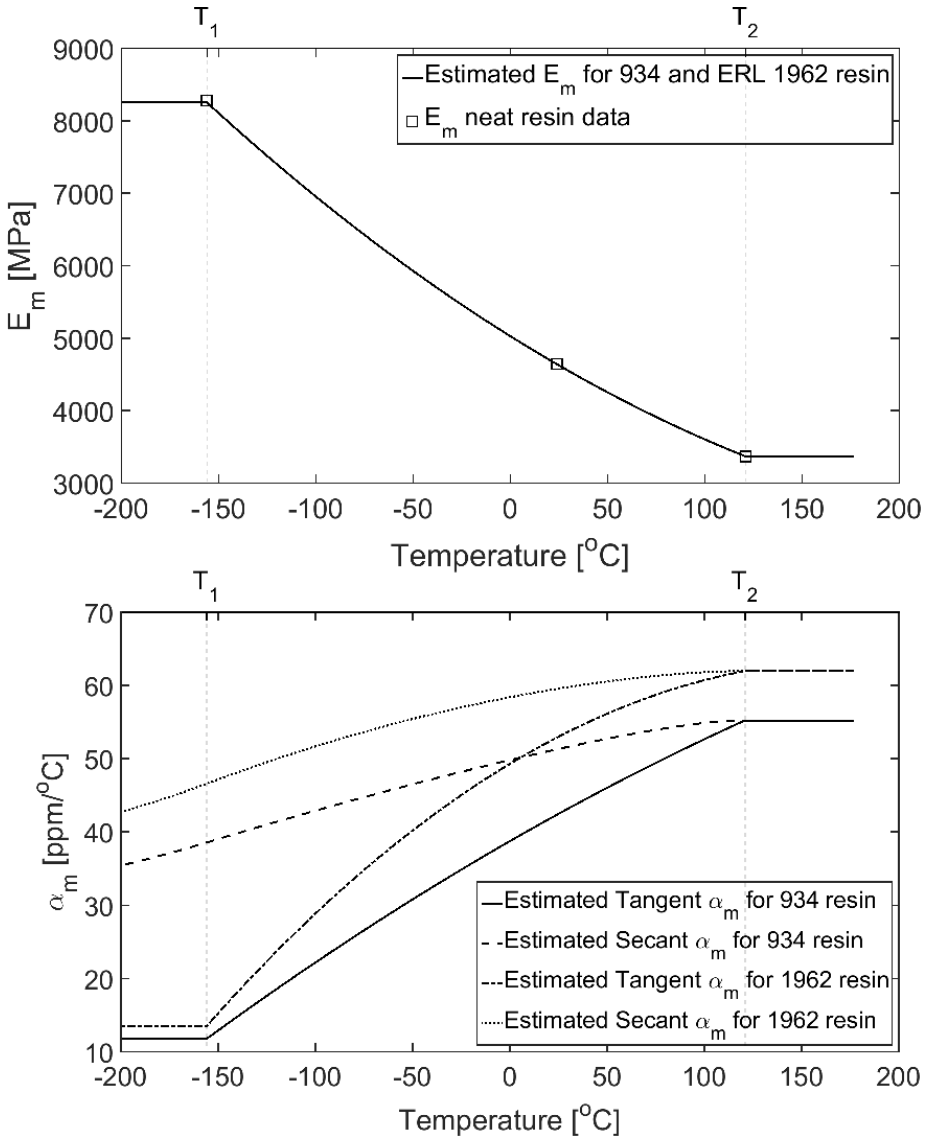

Figure 4. Estimated temperature-dependent modulus (top) and CTE (bottom) for Epoxy 934 and ERL 1962.

AS4 Fiber

The longitudinal modulus E_A of AS4 fiber is obtained from manufacturer data sheet [69,84]. The remaining elastic properties of AS4 fiber are back calculated from material system AS4/3501-6 using a set of experimental data at room (RT) and high (121^oC) temperature. The matrix properties E_m, ν_m of Epoxy 3501-6 at

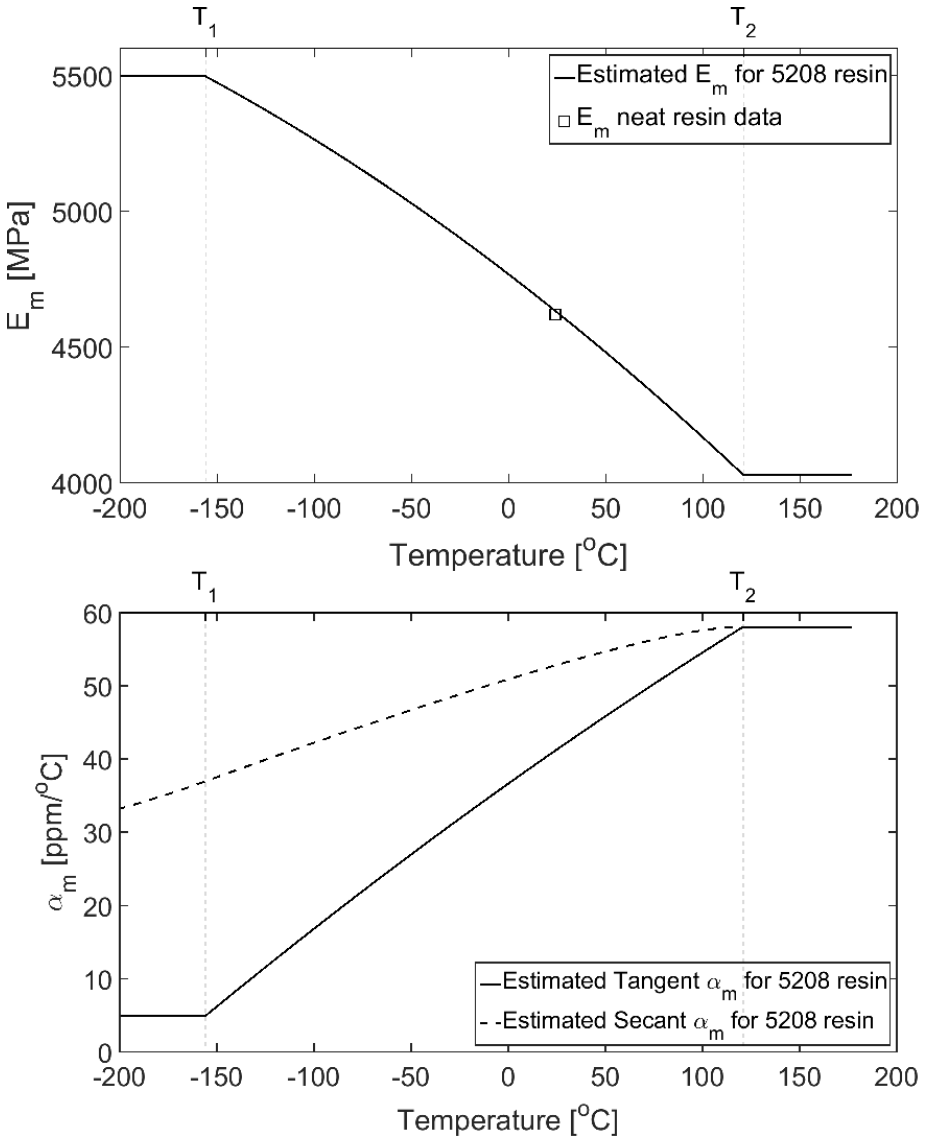

Figure 5. Estimated temperature-dependent modulus (top) and CTE (bottom) for Epoxy 5208.

room and high temperature are obtained from [78,79]. The rest of elastic fiber properties (E_T,G_A,ν_A,ν_T) are back calculated using set of experimental data at both temperatures by minimizing the error (6) between unidirectional lamina data ($E_1^d, E_2^d, G_{12}^d, \nu_{12}^d$) of AS4/3501-6 in [75] and predicted lamina properties ($E_1, E_2, G_{12}, \nu_{12}, \nu_{23}$) using PMM micromechanics. The methodology used is

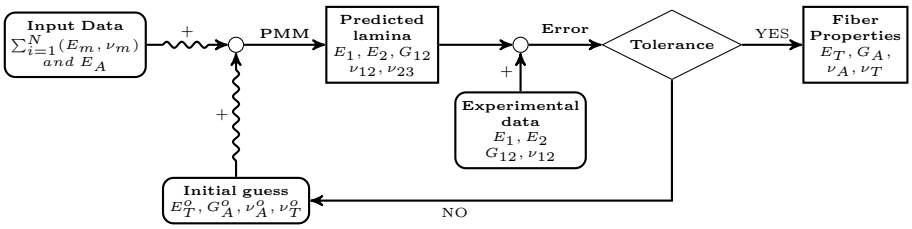

Figure 6. Back calculation method to obtain the fiber properties using set of experimental data at various temperatures (N).

shown in Figure 6 by a flowchart with tolerance[73] tol^x and $tol^{fun} = 10^{-8}$. The final AS4 fiber properties are reported in Table 1.

T300 Fiber

The longitudinal modulus E_A of T300 fiber is obtained from manufacturer data sheet[68]. The remaining elastic properties of T300 fiber are back calculated from material system T300/5208 at room temperature. The matrix properties E_m, ν_m, of Epoxy 5208 at room temperature are obtained from[85]. The rest of elastic fiber properties (E_T,G_A,ν_A,ν_T) are back calculated at room temperature by minimizing the error (6) between unidirectional lamina data ($E_1^d, E_2^d, G_{12}^d, \nu_{12}^d$) of T300/5208 in[12,13,70] and lamina properties ($E_1, E_2, G_{12}, \nu_{12}, \nu_{23}$) predicted with PMM. The procedure is illustrated in Figure 6 by a flowchart. The resulting properties for T300 fiber are reported in Table 1.

P75 Fiber

The average fiber modulus reported in the literature for (unsized) P75[21,81,84,86–91] and (sized) P75S[92] is $E_A = 517$ GPa. Using the longitudinal modulus $E_A = 517$ GPa and the properties of Epoxy 934 (Table 3), the rest of elastic properties (E_T, G_A, ν_A, ν_T) for P75 fiber are back calculated by minimizing (6) between unidirectional lamina data ($E_1^d, E_2^d, G_{12}^d, \nu_{12}^d$) of both P75/934 and P75/1962 available in[19,21,81,83,93] and lamina properties ($E_1, E_2, G_{12}, \nu_{12}, \nu_{23}$) predicted using PMM micromechanics. All the properties of P75 are back calculated using data from literature at room temperature. The procedure is illustrated in Figure 6 by a flowchart, with tolerance[73] tol^x and $tol^{fun} = 10^{-8}$. The resulting values are reported in Table 1.

Summary Constituent Properties

Once the fiber and matrix properties are adjusted, one can predict elastic lamina properties using PMM micromechanics and compare with available experimental data. Comparison between model predictions and experimental data for transverse modulus E_2 as a function of temperature are shown in

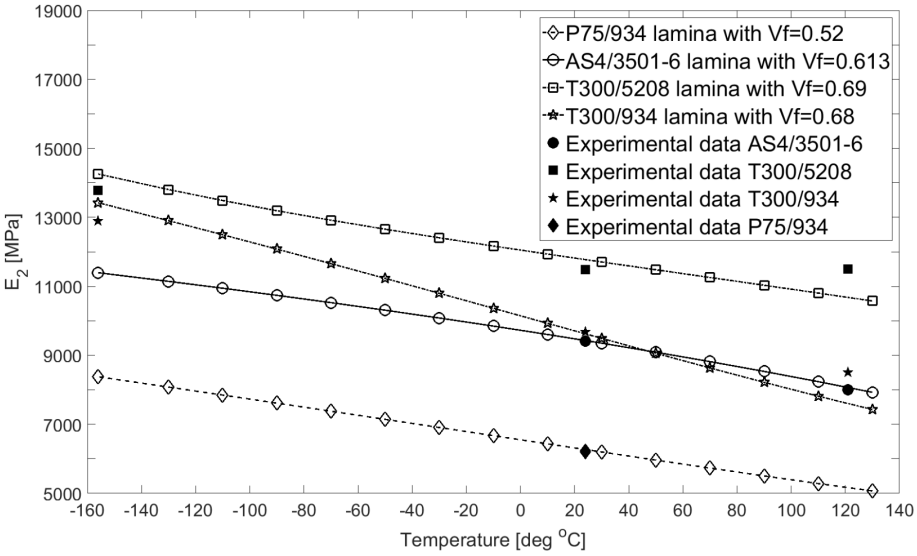

Figure 7. Comparison between predicted and experimental data of transverse modulus E_2 for P75/934, AS4/3501-6, T300/934, and T300/5208 lamina.

Figure 7. Comparison between model predictions and experimental data for in-plane shear modulus G_{12} as a function of temperature are shown in Figure 8.

Since fiber properties are assumed to be temperature-independent, the adjusted properties (E_T, G_T, ν_A, ν_T) are constant values that minimize the error between prediction and experimental data at several temperatures. In other words, the constant fiber properties are found in such a way that the deviation from predicted lamina data is as small as possible over the entire data set that may include data for several temperatures. On the other hand, matrix properties $E_m(T), \nu_m(T)$ are temperature-dependent, and thus adjusted to fit the temperature-dependent data. For matrix properties, different values of $E_m(T), \nu_m(T)$ are found at each temperature, and then fitted with the quadratic polynomial (5), as a function of temperature.

Coefficients of Thermal Expansion

The coefficients of thermal expansion (CTE) in the longitudinal and transverse directions of a lamina are defined as

$$\alpha_i = \frac{\partial \epsilon_i}{\partial T} \quad \text{with} \quad i = 1, 2 \tag{7}$$

where ϵ_i are the components of strain and T is the temperature. In this work α_i denote tangent CTEs (also called instantaneous CTE). The secant CTE is

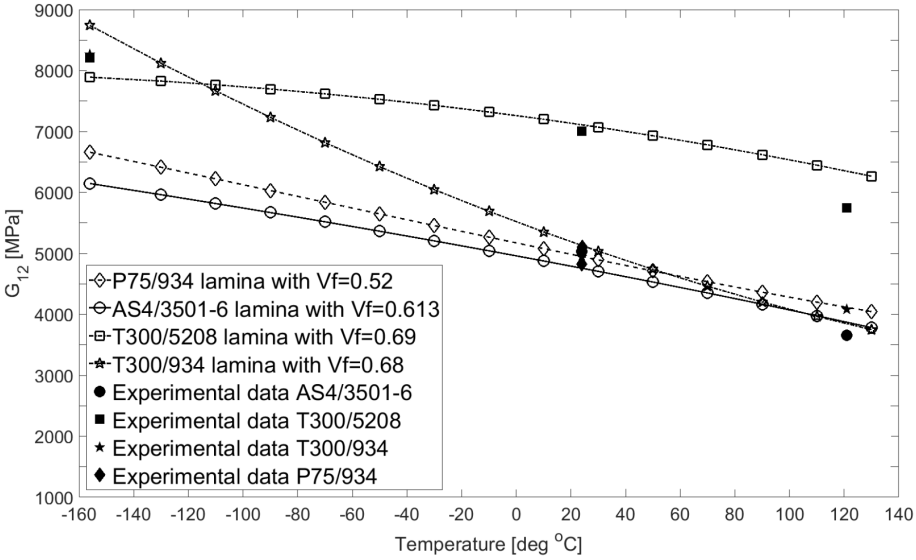

Figure 8. Comparison between predicted and experimental data of transverse modulus G_{12} for P75/934, AS4/3501-6, T300/934, and T300/5208 lamina.

defined as follows

$$\bar{\alpha}_i = \frac{1}{T - SFT} \int_{SFT}^{T} \alpha_i \, dT \tag{8}$$

where SFT is the stress free temperature. Equation (7) is useful because it directly relates the experimental thermal strain data of a unidirectional lamina with its CTE at any temperature without the need for specifying a reference temperature.

Levin[30,31] derived an exact solution for effective CTEs of a composite with two-phases: transversely isotropic (TI) fiber and isotropic matrix. Levin's Model (LM) relates volume average $\langle\cdot\rangle$ stresses and strains in a representative volume element (RVE) to obtain the effective CTEs as follows

$$\alpha_i = \alpha_{ij} = \langle\alpha_{ij}\rangle + (\alpha^f_{ij} - \alpha^m_{ij})(S^f_{ijkl} - S^m_{ijkl})^{-1}(S_{ijkl} - \langle S^f_{ijkl}\rangle) \text{ with } i = j \tag{9}$$

where S_{ijkl} are the elastic compliances, α_{ij} are the CTEs, and the subscripts f and m denote fiber and matrix, respectively. Equation (9) requires the effective elastic compliance S_{ijkl} as a function of temperature, which in this work is obtained using PMM. Hence, the elastic properties of the constituents as a function of temperature must be obtained before calculating the thermal properties. For isotropic matrix and TI fibers, $\alpha_{ij} = 0$ for $i \neq j$, and a single subscript suffices for all components of CTE.

Since the type of experimental data available varies from material to material, there are cases for which the CTE values for fiber α_A, α_T, and/or matrix $\alpha_m(T)$

are available from experimental data for fiber and/or matrix. However, in most cases they are not directly available, and thus they have to be adjusted by minimizing the error function

$$D_T = \frac{1}{N}\sqrt{\sum^{N}\left[\left(\frac{\alpha_i - \alpha_i^d}{\alpha_i^d}\right)^2\right]} \qquad \text{with } i = 1,2 \tag{10}$$

between experimental lamina CTE α_i^d data (available in the literature) and lamina CTE α_i predicted using (9). The subscripts $i = 1, 2$ denote longitudinal and transverse CTE, respectively, and N is the number of data values available. In order to give the same weight to all properties, the error function is normalized for each term.

Since longitudinal CTE α_1 is a fiber dominated property, the volume fraction is chosen to match the predicted longitudinal CTE with experimental data α_1^d at room temperature, which is available in the literature for all material systems considered in this study.

The CTE of matrix $\alpha_m(T)$ are always back calculated using the transverse lamina CTE α_2^d because the later is matrix dominated. Once the CTE $\alpha_m(T)$ are obtained at various temperatures using (10), a quadratic interpolation is carried out to obtain the polynomial's coefficients in (5). Manufacturer values of $\alpha_m(RT)$, if available, are used as initial guess for the error minimization algorithm.

Denoting by x the value of any CTE of interest, and by D_T the error (10), the value of property x is found when the error D_T is less than the function tolerance (i.e., error tolerance)[73] $tol^{fun} = 10^{-8}$ and the change in property Δx is less than the step size tolerance $tol^x = 10^{-8}$.

Since availability of data varies among material systems, not all material systems can be characterized exactly with the procedure described above. In fact, variations in the procedure are necessary to make use of the available data, which varies from material to material. In the following, five material systems (T300/5208, P75/934, T300/934, P75/1962, and AS4/3501-6) are characterized, illustrating how to adapt the proposed procedure to make best use of the available data.

Material system: T300/5208

The axial CTE α_A of T300 fiber is obtained from literature[3,94] and manufacturer data sheet[68]. Data for transverse CTE α_T of T300 fiber is not available. Therefore, for this material system only, the transverse CTE α_T of T300 fibers and temperature-dependent CTE $\alpha_m(T)$ of Epoxy 5208 are back calculated in three steps.

First, the transverse CTE α_T of T300 fiber and the RT CTE of the matrix $\alpha_m^0(RT)$ are back calculated by minimizing the error (10) using both the longitudinal and transverse lamina CTEs at RT. In this way, the transverse CTE α_T of T300 fiber and the RT CTE of the matrix $\alpha_m^0(RT)$ can be adjusted so that the lamina CTEs α_1, α_2, predicted using (9) match experimental CTEs

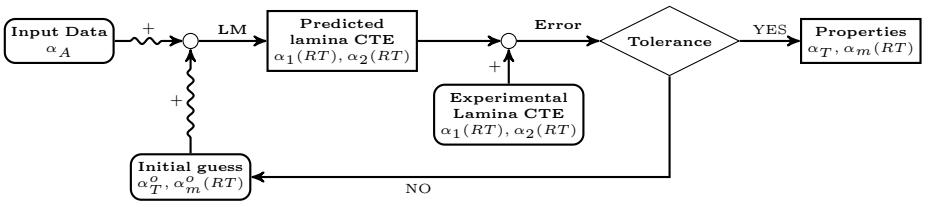

Figure 9. Back calculation method to obtain the fiber and matrix CTE values.

α_1^d, α_2^d, for T300/5208 lamina from [3,11,70]. The matrix CTE at RT from [85] is used as initial guess for $\alpha_m^0(RT)$. The methodology used is illustrated in Figure 9. Tolerances used [73] are $tol^x = tol^{fun} = 10^{-4}$. At the end of this first step, the CTEs of T300 fiber are reported in Table 1.

Second, the temperature-dependent CTE $\alpha_m(T)$ of Epoxy 5208 is back calculated at various temperatures (in the temperature range [120,-130 C]) by minimizing the error (10) between experimental lamina CTE in the transverse direction α_2^d for T300/5208 lamina in [3] and predicted lamina CTE α_2 using micromechanics (9). The procedure is illustrated by a flowchart in Figure 10. The matrix CTE previously calculated at room temperature $\alpha_m^0(RT)$ is used as initial guess. A schematic of the procedure is shown in Figure 10. Tolerance [73] used are $tol^x = tol^{fun} = 10^{-8}$.

Third, once the temperature-dependent CTE $\alpha_m(T)$ of Epoxy 5208 is calculated for a large number of temperature data points, the coefficients in (5) are obtained by a quadratic interpolation of those results. Then, the CTE of Epoxy 5208 as function of temperature is reported in Table 5.

Material system: P75/934 and T300/934

The CTE values α_A, α_T, of P75 fiber are obtained from literature and manufacturer data sheet [3,67,87,95]. Identical values were found in various literary resources and thus they are assumed to be valid for this study. Temperature-dependent CTE of Epoxy 934 could not be calculated using the data for P75/934 in [19] due to lack of experimental data points at cryogenic temperatures. Instead, data for material system T300/934 in [3] with temperature range $[121, -156^oC]$ is used to calculate the temperature-dependent CTE of Epoxy 934. Therefore, the temperature-dependent CTE $\alpha_m(T)$ of Epoxy 934 are back calculated at various temperatures by minimizing the error (10) between experimental lamina CTE in the transverse direction α_2^d for T300/934 lamina in [3] and predicted lamina CTE α_2 using micromechanics (9). The methodology used is illustrated in Figure 10 using tolerance [73] $tol^x = tol^{fun} = 10^{-8}$.

Once the matrix properties $\alpha_m(T)$ of Epoxy 934 are calculated for a large number of temperature data points, the coefficients in (5) are obtained by a quadratic interpolation of those results. The CTE of Epoxy 934 as function of temperature is reported in Table 3. The predicted values α_1, α_2, as a function

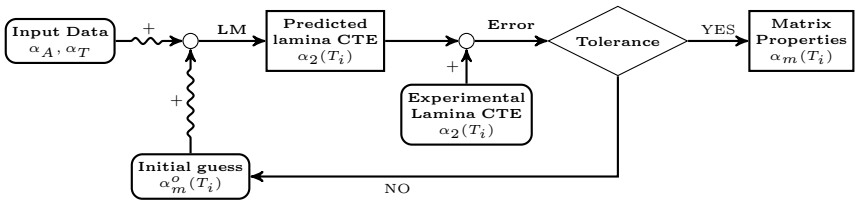

Figure 10. Back calculation method to obtain the matrix CTE at any temperature (T_i).

of temperature for P75/934 lamina are plotted in Section "Finite Element Analysis".

Material system: P75/1962

The temperature-dependent properties $\alpha_m(T)$ of Epoxy ERL 1962 are back calculated at various temperatures by minimizing the error (10) between experimental lamina CTE in the transverse direction α_2^d for P75/1962 lamina in[21,77], and lamina CTE α_2 predicted by micromechanics (9). The procedure is illustrated by a flowchart in Figure 10 using tolerance[73] $tol^x = tol^{fun} = 10^{-8}$.

The CTEs values of P75 fiber used in (9) are already reported in Table 1. Due to the availability of thermal strain data ϵ_i for this particular material system (P75/1962 lamina),[21,77] the CTE α_2^d data is calculated from thermal strain data ϵ_i using (7). Since ϵ_i data is quadratic in the temperature range [120,-150 C], the resulting CTE is also quadratic in the same temperature range. Once the temperature-dependent CTE $\alpha_m(T)$ of Epoxy ERL 1962 has been back calculated for a large number of temperature data points, the coefficients in (5) are obtained by a quadratic interpolation of those results. Then, the CTE of Epoxy ERL 1962 as function of temperature is reported in Table 4.

Material system: AS4/3501-6

The axial CTE α_A of AS4 fiber is obtained from manufacturer data sheet[69]. The temperature-dependent properties $\alpha_m(T)$ of Epoxy 3501-6 are taken from[6,17,96] in the temperature range [150,-90 C], which can be represented well by a linear function of temperature. Since the transverse CTE α_T of AS4 fiber is not available, it is back calculated by minimizing the error (10) between the predicted lamina CTE α_2 using micromechanics (9), and experimental lamina CTE α_2^d for AS4/3501-6 lamina available in[17]. The procedure used is shown in Figure 11 using tolerance[73] $tol^x = tol^{fun} = 10^{-8}$. The transverse CTE of AS4 fiber is reported in Table 1.

Summary CTE

Once the matrix CTE are adjusted, one can predict lamina CTE using (9) and compare with available experimental data (from sources cited above for each material system). Comparison between predicted lamina CTE using (9) and experimental data α_1^d, α_2^d is shown in Figures 12–13. The comparison in Figure 12

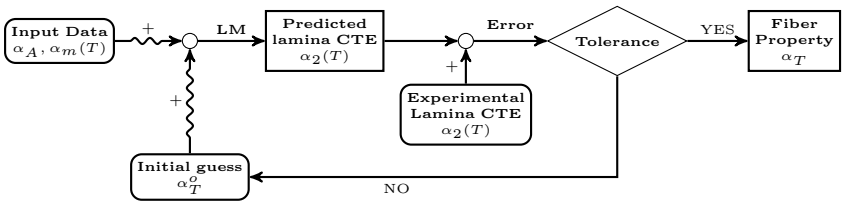

Figure 11. Back calculation method to obtain the transverse CTE of the fiber from transverse lamina CTE as function of temperature.

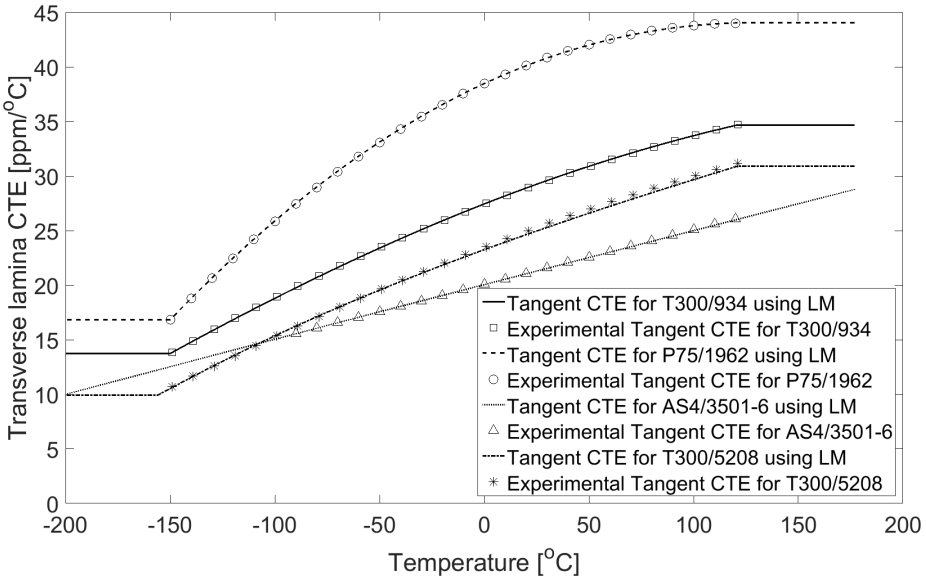

Figure 12. Comparison of transverse lamina CTE α_2 predicted with Levin's model (9) vs. experimental data for T300/934 with $V_f = 0.57$, AS4/3501-6 with $V_f = 0.67$, and P75/1962 with $V_f = 0.52$.

is excellent with α_2 in the range [5–45] 10^{-6}/C. In Figure 13, predicted and experimental values of α_1 do not match so well, except at room temperature. The deviation may be attributed to possible temperature-dependence of the transverse CTE of the fibers $\alpha_T(T)$, but such temperature dependency is impossible to ascertain without additional experimental data, which is not available.

Finite Element Analysis

In this section, the effective CTEs as function of temperature for a composite lamina are calculated using finite element analysis (FEA). The results are used to asses the accuracy of the micromechanics model (9) for CTE. A summary

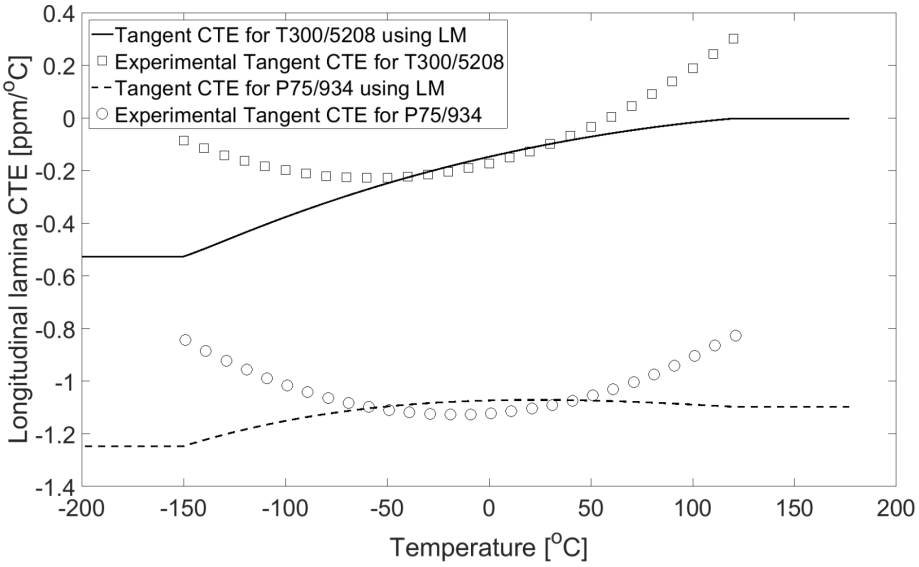

Figure 13. Comparison between longitudinal lamina CTE α_1 predicted with Levin's model (Eq. 9) and experimental data for T300/5208 with $V_f = 0.68$ and P75/934 with $V_f = 0.51$.

of the methodology is included, and comparison between micromechanics and FEA predictions is presented.

To obtain the effective CTEs for the whole temperature range, monotonic cooling is simulated from the stress free temperature (SFT) of the composite (approximated by the glass transition temperature T_g of the polymer) down to cryogenic temperatures (-200 C).

To represent a transversely isotropic lamina with 3D solid elements, the microstructure is assumed to have the fibers arranged in an hexagonal array, and from that microstructure a representative volume element (RVE) limited by a cuboid is represented, as it can be seen in Figures 6.3–6.5 in[50]. The dimensions of the RVE are calculated to achieve the desired volume fraction V_f, as explained in Example 6.2 in[50].

Periodic boundary conditions (PBC) are imposed to the RVE in order to enforce continuity of displacements. To avoid over constraining at edges and vertices, master nodes (MN), one for each face of the RVE in x_1, x_2, and x_3 directions, are used to couple the DOF through constraints equations. The BCs thus become

$$\begin{array}{cc} \text{symmetry} & \text{uniform displacements} \\ u_1(0,x_2,x_3)=0; & u_1(a_1,x_2,x_3)=u_1^{MN_{X_1}} \\ u_2(x_1,0,x_3)=0; & u_2(x_1,a_2,x_3)=u_2^{MN_{X_2}} \\ u_3(x_1,x_2,0)=0; & u_3(x_1,x_2,a_3)=u_3^{MN_{X_3}} \end{array} \tag{11}$$

where MN_{X_1}, MN_{X_2} and MN_{X_3} are the master nodes (reference points) in x_1, x_2 and x_3 directions, respectively. The RVE occupies the volume with dimensions: $0 \leq x_1 \leq a_1,\ 0 \leq x_2 \leq a_2,$ and $0 \leq x_3 \leq a_3$. The MNs are tied to surfaces defined by $x = a_1, y = a_2, z = a_3$. No displacements or loads are specified at the MN, so that the RVE is free to expand/contract with thermal expansion but subject to compatibility conditions with the surrounding continuum.

The temperature-dependent properties of the matrix E_m, ν_m, α_m, are defined as a set of N temperature-property data pairs as (T_1, P_1), (T_2, P_2),..., (T_N, P_N). The values are obtained using (5) and Tables 2–5. These values are discretized with $\Delta T = 1$ C to simplify the computations and interpretation of results. Outside the range [-156,120] for which experimental data is available, the properties of the matrix are assumed to be constant and equal to the first (or last) experimental data pair (Figures 4,5).

Two python scripts (`'ParameterIntegrator.py'` and `'Excelproperties.py'`) are used to create the input property tables for the matrix material. *All Python scripts are available as supplemental materials on the publisher's website.* Since the matrix properties are defined by *piece-wise* functions (Figures 4,5), the resulting lamina properties are also *piece-wise* functions (Figures 14–16). The transversely isotropic properties of the fibers are assumed to be constant over the entire temperature range. Curing-induced shrinkage of the epoxy resin is not taken into account.

FEA analysis was performed with Abaqus 6.14, using small displacement, linear elastic material, and 3D elements C3D8R. A Python script (`'LaminaName.py'`) is used to generate the FEA model. A mapped mesh was constructed providing identical mesh on opposite surfaces. The PBC are implemented as constraints equations between master nodes and surfaces with normals along the x, y, z directions, respectively. A Python script (`'PBC.py'`) is used to automate such process. Symmetric BC were applied to surfaces defined by $x = 0, y = 0, z = 0$.

Finally, a Python script (`'Epsilonrecover.py'`) is used to calculate the accumulated thermal strains at temperature T via volume averages from mesh elements j as

$$\epsilon(T) = \frac{1}{V_{RVE}} \int_{V_{RVE}} \hat{\epsilon}(x, y, z)\, dV = \frac{1}{V_{RVE}} \sum_{j=1}^{elements} \hat{\epsilon}^j\, V_i^j \tag{12}$$

Computational micromechanics is used in this section as described in Ch. 6 in[50]. In this way, constituent properties can be assigned separately to the constituents (fiber and matrix) and the FEA model can be subjected to a variation of temperature. Then, FEA calculates the strain $\hat{\epsilon}(x, y, x)$ at all Gauss integration points inside the representative volume element (RVE) and the average strain over the RVE is easily computed as in (12).

The tangent CTE $\alpha(T)$ is a function of temperature in (7) and the secant CTE $\bar{\alpha}(T)$ is also a function of temperature (8), using the stress-free temperature (SFT) as reference temperature. For each increment of temperature T, Abaqus

calculates the accumulated strain in terms of the secant CTE (as stated in [97]) i.e.,

$$\epsilon^{acc}(T) = \bar{\alpha}(T) \times (T - SFT) \tag{13}$$

and the user has to calculate tangent CTE by differentiation in (7).

Both α_m and $\bar{\alpha}_m$ are smooth continuous functions in the interval $[T_1, T_2]$ for which experimental data exists (see labels T_1, T_2 in Figs. 4 and 5), but they are constant outside that range, i.e. in the ranges $[-200, T_1]$ and $[T_2, SFT]$. Recall that the properties are assumed constant outside the range for which experimental data exist, as shown in Figures 4–5. Since a piece-wise function is not differentiable at the transition points T_1 and T_2, (7) cannot be used and the tangent CTE at those temperatures is undefined.

To solve the indetermination, we propose to provide Abaqus with the tangent rather than the secant, i.e., substitute $\alpha(T)$ for $\bar{\alpha}(T)$ in (13). In this situation, Abaqus calculates a fictitious strain $\epsilon^{acc*}(T)$, as per the following equation

$$\epsilon^{acc*}(T) = \alpha(T) \times (T - SFT) \tag{14}$$

which is not the actual accumulated strain but a fictitious value. However, dividing this fictitious value by the temperature interval $(T - SFT)$, i.e., rewriting (14) as

$$\alpha(T) = \frac{\epsilon^{acc*}(T)}{(T - SFT)} \tag{15}$$

the desired result is obtained, namely the tangent CTE, while avoiding the differentiation (7), and thus a potential error is eliminated.

Using the aforementioned procedure, effective CTEs α_1, α_2 are calculated using FEA and then compared with experimental data and with predicted lamina CTE using (9) for all the material systems considered in this study. Comparison between FEA-calculated and experimental values α_1 and α_2 at room temperature from [3,11,19,21,70,96] are reported in Table 6 and 7. The predictions compare very well with experimental data for all the material system studied. The only anomaly observed is for longitudinal lamina CTE for T300/934 shown in Table 6, which may be due to a slight deviation in the fiber volume fraction. Longitudinal lamina CTE is very sensitive to fiber volume fraction. For example, just increasing fiber volume fraction by 2%, the predicted value drops to 0.069 10^{-6}/C, thus reducing the difference.

Comparison between predicted lamina CTE using (9) and FEA is shown in Figures 14–16. The CTE predictions by both methods are very close. Longitudinal CTE is compared in Figure 14 and transverse CTE is compared Figures 15–16. It can be seen that Levin's model is as accurate as FEA. Since Levin's model is analytical, it is then used for all remaining calculations in this work.

Table 6. Comparison of experimental and FEA-calculated longitudinal lamina CTE α_1 at 24 C.

Material System	V_f [%]	Experimental α_1 [10^{-6}/ C]	FEA α_1 [10^{-6}/ C]	% Error	Reference
T300/5208	68	-0.113	-0.113	0.1	[3] & Fig. 13
T300/5208	70	-0.166	-0.163	1.8	[11,70]
T300/934	57	-0.001	0.151	111.9	[3]
P75/934	51	-1.051	-1.071	1.8	[19]
P75/1962	52	-0.987	-0.984	0.3	[21]
AS4/3501-6	67	-	-0.194	-	[96] & Fig. 11

Table 7. Comparison of experimental and FEA-calculated transverse lamina CTE α_2 at 24 C.

Material System	V_f [%]	Experimental α_2 [10^{-6}/ C]	FEA α_2 [10^{-6}/ C]	% Error	Reference
T300/5208	68	25.236	24.960	1.1	[3] & Fig. 13
T300/5208	70	23.327	23.752	1.7	[11,70]
T300/934	57	29.340	29.170	0.6	[3]
P75/934	51	34.531	34.061	1.4	[19]
P75/1962	52	40.405	40.493	0.21	[21]
AS4/3501-6	67	21.212	21.335	0.6	[96] & Fig. 11

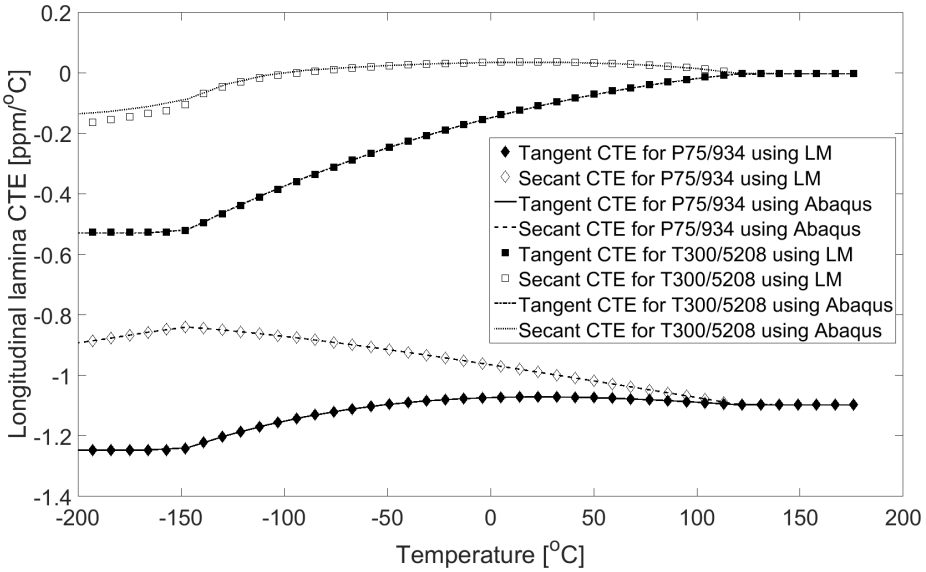

Figure 14. Comparison micromechanics and FEA predictions of tangent and secant longitudinal CTE α_1 for P75/934 ($V_f = 0.51$) and T300/5208 ($V_f = 0.68$).

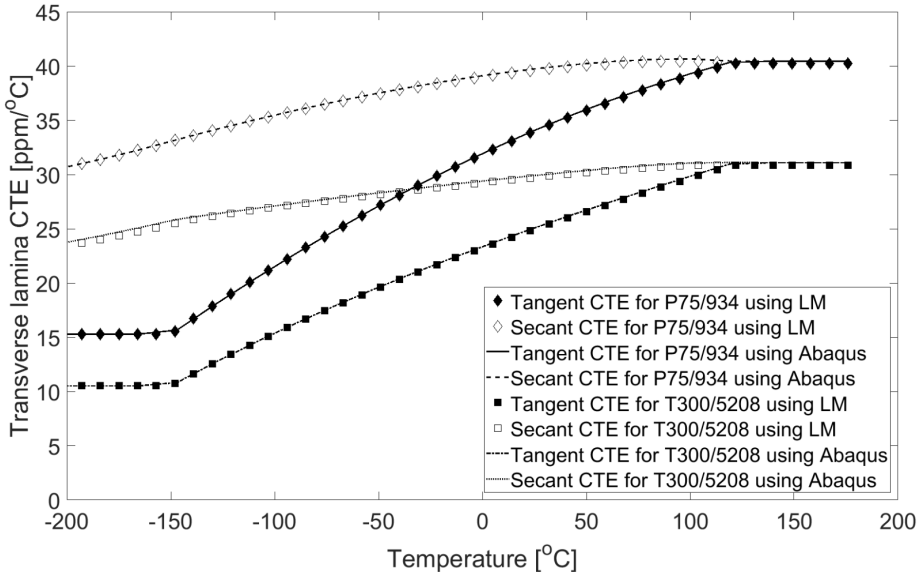

Figure 15. Comparison micromechanics and FEA predictions of tangent and secant transverse CTE α_2 for P75/934 ($V_f = 0.51$) and T300/5208 ($V_f = 0.68$).

Critical Energy Release Rates

To a first approximation, intralaminar cracking of unidirectional laminated composites can be described by the modified Griffith's criterion [98,99] for brittle materials undergoing small plastic deformations and blunting of the crack tip. Refinements to this approximation increase the complexity of the model to achieve more accuracy [100]. However, the modified Griffith's criterion has been extensively validated for predicting initiation and accumulation of damage in the form of intralaminar cracks for a variety of material systems [47,59,61,83,101,102]. As it was commented in the Introduction, polymers become brittle at low temperature, and thus the onset and development of new cracks can be described by Linear Elastic Fracture Mechanics, whose crack initiation is controlled by fracture toughness K_{Ic}. Once the crack starts, it suddenly propagates up to

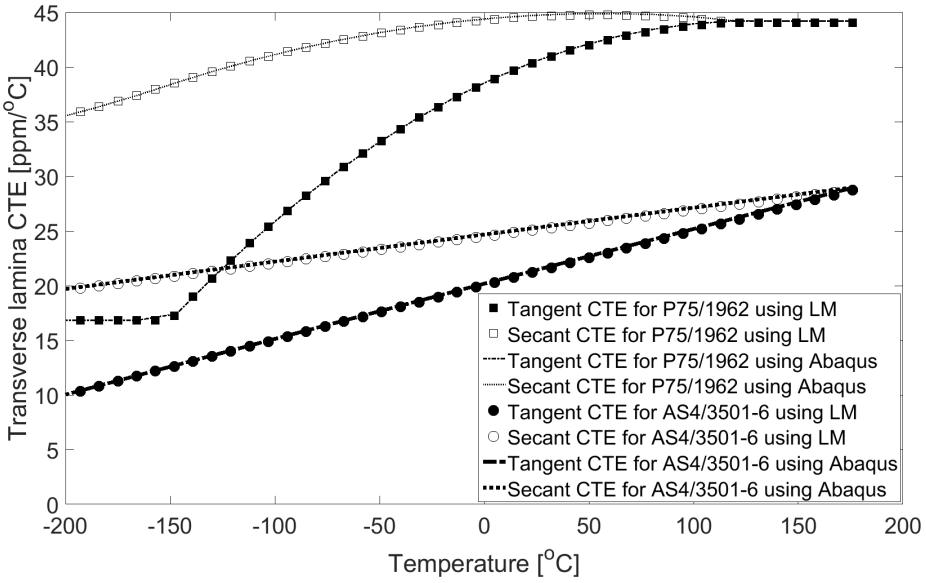

Figure 16. Comparison between micromechanics and FEA predictions of tangent and secant transverse CTE α_2 for P75/1962 ($V_f = 0.52$), and AS4/3501-6 ($V_f = 0.67$).

adjacent laminas. Assuming the width much larger than the thickness (plane-strain), the critical ERR G_{Ic} can be related to the fracture toughness as follows

$$G_{I_c} = \frac{K_{Ic}^2}{E}(1-\nu^2) \tag{16}$$

$$K_{Ic} = \sigma_t \alpha \sqrt{\pi a} \tag{17}$$

where E is the Young's modulus, ν the Poisson's ratio, σ_t the tensile strength, α a parameter to account for the geometry of the specimen, and a the crack length.

Looking at (16), it would appear that G_{Ic} should be temperature dependent because E and ν are temperature dependent. In fact E increases with cooling (Figure 7) while ν may decrease slightly or remain virtually constant. However, it remains to ascertain the temperature dependence of K_{Ic}. If both E and K_{Ic}^2 were to increase/decrease at the same rate, then G_{Ic} would be virtually constant.

According to the literature, K_{Ic} generally increases at cryogenic temperatures for a large variety of polymers[39,103–105] and specifically for epoxy[42,44,106,107]. The physical phenomenon that can explain this increment is reported in[36,107,108]. On one hand, the specific heat conduction of plastics is very small at low temperature[38,40,106,109,110], behaving as insulating material. Thus, heat conduction is impaired and the crack tip, which is subject to approximately adiabatic conditions. On the other hand crack propagation is unstable, reaching high speeds, up to 1/3 of the transverse sound velocity in brittle materials such as epoxy at low and cryogenic temperatures. Due to crack propagation

speed, friction, chain scissions, and high-rate deformation, heat is generated that causes temperature to rise at the crack tip under adiabatic conditions. High temperature induces a plastic zone at the crack tip that absorbs energy and arrests the crack until additional external load and deformation increases the ERR sufficiently to start the crack again. This is corroborated by arrest lines[40] that can be observed, which are left behind the path followed by the crack propagating through the material in this fashion. This provides justification for the increment of K_{Ic} with cooling.

The rate of growth of K_{Ic} with cooling could be ascertained from (17) in terms of the tensile strength σ_t, which increases at low temperatures[106], while the tensile strain ϵ_t decreases[37–40]. However, lacking experimental data for K_{Ic} and σ_t at low and cryogenic temperatures for the polymers of interest (Epoxies 3501-6, 5208, 934, and 1962), an alternative method is needed to estimate the critical ERR G_{Ic}. Therefore, in this work, the critical ERR values are adjusted so that the DDM damage model predicts the same crack density as available experimental crack density data λ^d by minimizing the following error D function

$$D = \frac{1}{N}\sqrt{\sum_{j=1}^{N}\left(\lambda_j - \lambda_j^d\right)} \tag{18}$$

where N is number of data points at a given temperature, and λ_j is the crack density.

In order to study the temperature dependence of G_{Ic}, two different approximations are used in this section. In the first approximation, the critical ERR G_{Ic} is assumed to be temperature dependent and thus adjusted by minimizing the error D (18) at each temperature for which experimental data is available. Then, a polynomial such as (5) is adjusted though the values of G_{Ic} obtained at those temperatures. To adjust a polynomial over the temperature range of interest [-200,180 C], only data for material systems that have been tested at several temperatures over that range can be used. For example, data that only exists for a single temperature cannot be used to characterize temperature-dependence.

In the second approximation, the critical ERR G_{Ic} is assumed to be temperature independent (constant). Therefore, all data λ^d can be used regardless of whether data from a given source is available for just one or for multiple temperatures. Furthermore, if it could be shown that a constant (temperature independent) value of critical ERR G_{Ic} is sufficiently accurate to predict crack density vs. temperature, then the amount of testing needed to characterize a material system could be reduced with respect to G_{Ic} being a function of temperature.

The specific details of both procedures are described next.

Assuming temperature-dependent G_{Ic}, the critical ERR G_{Ic} is adjusted by minimizing the error D (18) between the predicted crack density λ and experimental crack density data λ^d for each temperature for which experimental data is available[70,76,82,83]. Prediction of crack density is performed using the Discrete Damage Mechanics (DDM) formulation (Ch. 8 in[23]).

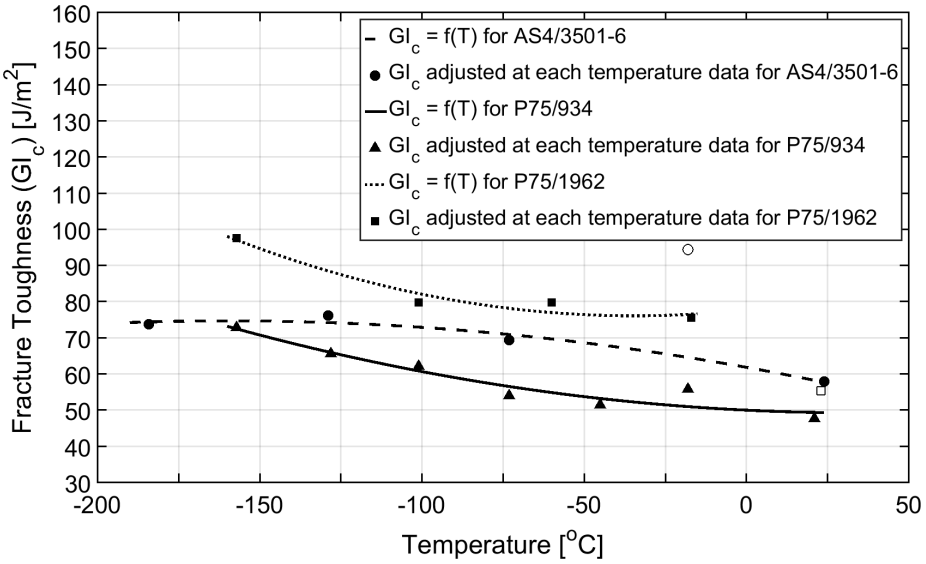

Figure 17. G_{Ic} vs. temperature for P75/934 (Vf =0.65), P75/1962 (Vf =0.52), and AS4/3501-6 (V_f =0.64). Two outliers data, at -18 C for AS4/3501-6 and at -21 C for P75/1962, not used.

Table 8. Critical ERR G_{Ic} [J/m^2], temperature [°C], see eq. (5).

	Temp. dependent				Temp.
Material	P_a	P_b	P_c	Range [^oC]	independent
P75/934	50.0561	-4.3006 10^{-2}	6.3749 10^{-4}	[-160,20]	53.4050
P75/1962	77.8054	9.6211 10^{-2}	1.3948 10^{-3}	[-160,-15]	84.4808
AS4/3501-6	61.9052	-1.6097 10^{-1}	-5.0412 10^{-4}	[-190,20]	68.0664

G_{Ic} values for material systems P75/934 $[0_2/90_2]_S$, P75/1962 $[0_2/45_2/90_2/-45_2]_S$, and AS4/3501-6 $[0_4/45_4/90_4/-45_4]_S$, obtained at discrete temperatures are then fitted with a quadratic polynomial as shown in Figure 17. Material system T300/5208 $[0_2/90_2]_S$ undergoes negligible cracking until -156 C[70], so it is not included in the figure. The coefficients of the quadratic polynomial (5) for temperature-dependent G_{IC} are reported in Table 8.

Some outlier data points are reported for AS4/3501-6 and P75/1962 around -18 C and 23 C, respectively. These outliers correspond to data with a large scatter so they were not used in this study. For all cases, a quadratic interpolation was found to accurately represent $G_{Ic}(T)$ as a function of temperature. According to Figure 17, G_{Ic} at low temperature increases between 26.91 % and 39.46 % with respect RT.

Assuming temperature-independent G_{Ic}, the critical ERR G_{Ic} is adjusted using all sets of experimental crack density λ^d available. Values of constant G_{Ic} are reported on the last column in Table 8. A comparison between

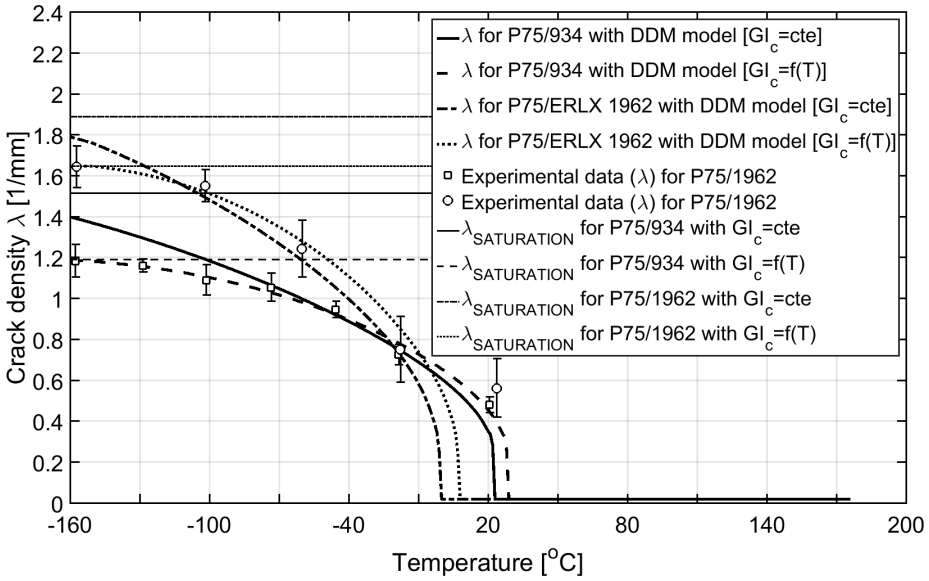

Figure 18. Crack density data vs. Temperature for laminates $[0_2/90_2]_s$ P75/934 and $[0_2/45_2/90_2/-45_2]_s$ P75/1962.

the predicted crack density and experimental data subjected to monotonic cooling is shown in Figures 18–19 using both constant G_{Ic} and temperature-dependent $G_{Ic}(T)$. Only constant G_{Ic} was used for T300/5208 due to lack of experimental data at low temperatures for this material system. However, temperature dependence of the constituents is taken into account for all cases. Prediction of crack density vs. temperature are quite good with either constant G_{Ic} or temperature-dependent G_{Ic} for all materials systems except P75/934 and P75/1962, for which accuracy at cryogenic temperature improves when temperature-dependent G_{Ic} is used.

For P75/934, P75/1962, and T300/934, the experimental data was measured at the edge of the specimens[70,76,82,83]. For AS4/3501-6, experimental data was measured at both the edge and the interior of specimens[76]. G_{Ic} is calculated from interior data for AS4/3501-6 but edge data is also shown in Figure 19 for comparison. Interior data was used, if available, because the agreement between predicted and experimental crack density is better, and X-ray data (used to detect interior cracks) is usually more reliable that optical edge inspection.

Saturation crack density is here defined as the asymptotic value of crack density as temperature approaches extremely low temperature. Saturation crack density is shown in Figures 18–19 to illustrate the expected behavior at lower temperatures than those for which experimental data is available.

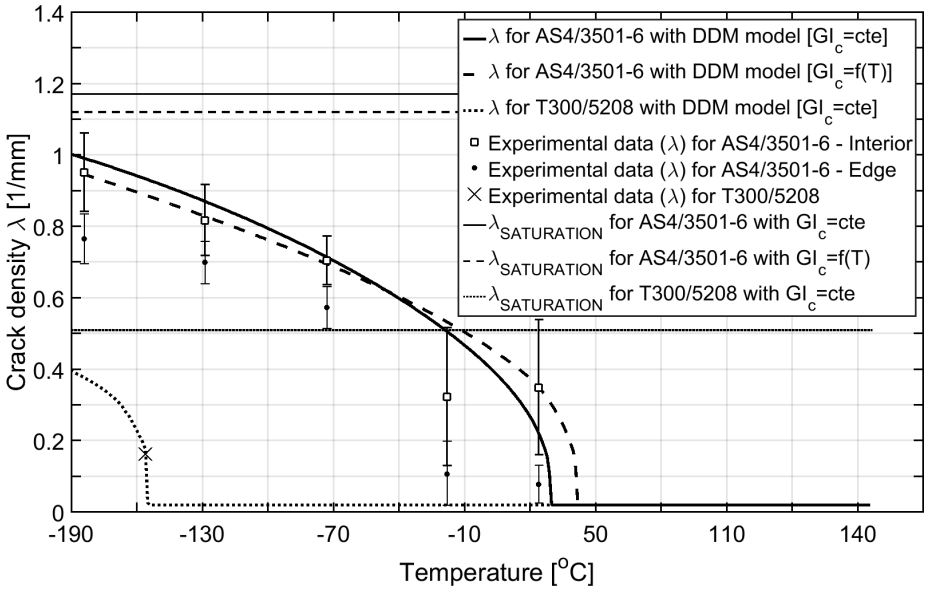

Figure 19. Crack density data vs. Temperature for laminates $[0_4/45_4/90_4/-45_4]_s$ AS4/3501-6 and $[0_2/90_2]_s$ T300/5208.

It can be seen in Figures 18–19 that the rate of damage with cooling, defined as

$$\dot{\lambda} = -\frac{\partial \lambda}{\partial T} \tag{19}$$

decreases over the whole temperature range. That is, less and less damage is induced by the same decrement of temperature ΔT as the temperature decreases. This is due to four factors. First, damage accumulation reduces the transverse stiffness E_2, thus larger strains can occur at the same stress level in the cracking lamina. Second, E_2 increases with cooling (Figure 7), which works opposite to the previous effect. Third, the transverse CTE α_2 decreases with cooling (see Figures 15–16), so larger reductions of temperature can be tolerated with the same increment of damage. When these three effects are combined, it seems that constant G_{Ic} is the answer, with the reduction of damage rate at lower temperature being captured quite well by the model, although some differences can be observed at cryogenic temperature for P75/934 and P75/1962. The fourth factor is the increase of critical ERR with cooling depicted in Figure 17, where it can be seen that the temperature dependence of G_{Ic} is more pronounced for P75/934 and P75/1962. For the other materials systems, the temperature dependence is less pronounced and thus predictions of crack density with constant G_{Ic} are better. Note that an increase of G_{Ic} with cooling (Figure 18) further reduces the rate of damage at lower temperatures.

Conclusions

Since elastic and CTE properties of polymers are temperature-dependent, they induce temperature-dependency on all the effective properties of laminas and laminates. However, the temperature dependency of fiber-dominated properties is small because the fiber-properties are virtually independent of temperature.

The temperature dependence of polymer properties can be accurately represented by a quadratic function and in some cases the variation is so slight that a linear function suffices.

Although the experimental data is scarce, non-existent in some cases, and displays great scatter in other cases, a systematic procedure was developed and applied to extract in situ properties for both fibers and polymers encompassing four composite material systems while taking into account their temperature dependence.

Finite element analysis confirms the accuracy of the analytical micromechanics model selected for this study. Once the fiber and polymer are characterized, micromechanics allows computation of all lamina effective properties for the temperature range of interest. However, care should be taken not to extrapolate outside the temperature range of the experimental data used for material characterization, particularly when nonlinear equations are used to model the data. Predictions outside this range are thus made assuming constant values for all properties outside the temperature range of the experimental data.

When laminates are mechanically loaded, damage initiation and accumulation up to crack saturation are characterized by two values of critical ERR in modes I (opening) and II (shear). However, cooling of quasi-isotropic laminates produces only mode I cracking because the thermal contraction is the same in every direction, and cross-ply laminates crack in mode I only because there is no shear induced. Therefore, only G_{IC} was characterized and used in this study.

The critical ERR is easily obtained by minimizing the error between crack density prediction and available data. A constant value of critical ERR produces satisfactory approximation of crack density vs. temperature. To eliminate the small discrepancy on saturation crack density at cryogenic temperature requires adjusting the critical ERR with a quadratic equation. From a practical point of view, being able to produce satisfactory estimates of damage with a constant value of critical ERR is advantageous because it reduces the amount of experimentation needed to adjust the critical ERR.

Some of the experimental crack-density data is inconclusive about crack saturation for some material systems, namely AS4/3501-6 and T300/5208. In other words, for those material systems the temperature at which data is available is not low enough to show crack density leveling off. However, model predictions clearly show that crack saturation is likely in all cases. This is because the critical ERR does not change much with cooling, but transverse CTE drops significantly with cooling (Figures 15–16), thus depriving the system from the main driver for thermo-mechanical matrix cracking.

Supplemental material

Supplemental material is available on the publisher's website. A brief explanation about its use is included in this section.

First, some libraries such as Numpy, Math and Xlsxwriter are needed to perform elemental and advanced math operations required to run the attached Python Scripts. Installation of these or other libraries to extend Abaqus functionality is described in detail on [111]. Note that the *Numpy* or *Math* library are already installed in Abaqus by default, so these library versions cannot be changed. However, *Xlsxwriter* library is required to handle or create new tables using an Excel file extension, and it must be installed as follows:

- Determine the Phyton *version* (≫ import sys) using the windows command from the installed Abaqus version.
- Install the correct Python version determined previously. Onwards, any necessary library to be used by Abaqus except *Numpy* or *Math* library must be first installed in the Python folder.
- Install the *Xlsxwriter* module in the Python folder. Check *Xlsxwriter* compatibility in [112] for Python version installed. Once the *Xlsxwriter* library is already installed in Python folder, it must be copied/moved to the Abaqus library folder, similar to the following path: `C:\SIMULIA\Abaqus\6.14-2\tools\SMApy\python2.7\Lib\site-packages`. This procedure can be followed for any other type of library if needed.

Once all the libraries needed are properly installed, the FEA model can be run keeping in the same folder the following scripts:

a) *LaminaName.py*: creates a RVE with identical mesh through the thickness in order to apply the PBC as well as material properties, steps, thermal loads and job.

b) *PBC.py*: a function script which detects a basic geometry (it can be another one such as cube, polygonal shape,...) and creates the PBC constraints. This script is good because you can apply PBC independently of the RVE shape (may be not to much complicate).

c) *ParameterIntegrator.py*: special function with 4 sub-functions which can calculate the value of a function, the integral of a second order polynomial, and the accumulated thermal strain given the tangent lamina CTE, typically as one can find in the literature.

d) *ExcelProperties.py*: script to obtain an Excel table with the temperature-dependent properties

e) *Epsilonrecover.py*: script to obtain the accumulated thermal strain once the FEA model has been submitted.

The FEA model can be run as follows:

- Run this script with the constituent properties and settings
  a) Set your work directory and run *LaminaName.py*
  b) Select 'Part-1' in Part section to see the RVE
  c) Go to 'Interaction' section to check that all the PBC have been created. The PBC must be shown as small yellow circles.
  d) Go to 'Job' section and submit the Job
- Once 'Job-1' has been completed successfully, run the 'Epsilonrecover.py' script
- Wait until appear the message 'All calculations finished', on Message Area
- In current folder, the excel file with the accumulated thermal strain should appear as 'Alpha.xlsx'
- The excel file with matrix properties is optional. You can run 'Excelproperties.py' once *LaminaName.py* script has been run.

Funding

This research received no specific grant from any funding agency in the public, commercial, or not-for-profit sectors.

Conflict of interest

The Authors declare that there is no conflict of interest.

References

1. E. M. Silverman. Space environmental effects on spacecraft: Leo materials selection guide. Technical Report NSA1-19291, NASA Langley Research Center, Hampton, VA, United States, August 1995.
2. E.G. Wolff. Stiffness-thermal expansions relationships in high modulus carbon fibers. *Journal of Composite Materials*, 21:81–97, 1987.
3. David E. Bowles. Micromechanics analysis of space simulated thermal deformations and stresses in continuous fiber reinforced composites. Technical Report 90N21140, NASA, 1990.
4. D.F. Adams. Finite element micromechanical analysis of a unidirectional composite including longitudinal shear loading. *Journal of Computers and Structures*, 18(6):1153–1165, 1984.
5. T.R. King, D.M. Blackketter, D.E. Walrath, and D.F. Adams. Micromechanics prediction of the shear strength of carbon fiber/epoxy matrix composites: The influence of the matrix and interface strengths. *Journal of Composite Materials*, 26(4):558–573, 1992.
6. D.F. Adams. A micromechanics analysis of the influence of the interface on the performance of polymer-matrix composites. *Journal of Reinforced Plastics and Composites*, 6(1):66–88, 1987.
7. Choi Sukjoo and B.V. Sankar. Micromechanical analysis of composite laminates at cryogenic temperature. *Journal of Composite Materials*, 0:1–15, 2005.

8. Y.Y. Ran Zhiguo, Q.Z. Li Jianfeng, and Yang L. Determination of thermal expansion coefficients for unidirectional fiber-reinforced composites. *Chinese Journal of Aeronautics*, 27(5):1180–1187, 2014.
9. X. Song, Y Chen, S. Chen, E. J. Barbero, E. L. Thomas, and P. Barnes. Significant enhancement of electrical transport properties of thermoelectric ca3co4o9+d through yb doping,. *Solid State Comm.*, 152(16):1509–1512, 2012.
10. X. Song, D. McIntyre, X. Chen, E.J. Barbero, and Y. Chen. Phase evolution and thermoelectric performance of calcium cobaltite upon high temperature aging. *Ceramics International*, 41(9, Part A):1106911074, 2015.
11. M.W. Hyer, C.T. Herakovich, S.M. Milkovich, and J.S. Short. Temperature dependence of mechanical and thermal expansion properties of T300/5208 graphite/epoxy. *Composites*, 14(3):276–280, 1983.
12. S. M. Milkovich and C.T. Herakovick. Temperature dependence of elastic and strength properties of T300/5208 graphite-epoxy. Technical report, NASA-CR-173616, 1984.
13. David E Bowles. Effect of microcracks on the thermal expansion of composite laminates. *Journal of composite materials*, 18(2):173–187, 1984.
14. R.Y. Kim, A.S. Crasto, and G.A. Schoeppner. Dimensional stability of composite in a space thermal environment. *Science and Technology*, 60(12):2601–2608, 2000.
15. D.F. Adams, R.S. Zimmerman, and E.M. Odom. Polymer matrix and graphite fiber interface study. Technical Report NASA-CR-165632, NASA, 1985.
16. R.R. Johnson, M.H. Kural, and G.B. Mackey. Thermal expansion properties of composite materials. Technical Report NASA-CR-177357, NASA, 1981.
17. D.S. Cairns and D.F. Adams. Moisture and thermal expansion properties of unidirectional composite materials and the epoxy matrix. *Journal of Reinforced Plastics and Composites*, 2(4):239–255, 1983.
18. JR.M. Michno. High modulus composite properties. In *2nd Aerospace Maintenance Conference*, pages 126–131, 1986.
19. S.S. Tompkins. Thermal expansion of selected graphite-reinforced polyimide-, epoxy-, and glass-matrix composites. *Journal of Thermophysical Properties and Thermophysics and its Applications.*, 8:119–132, 1987.
20. S.M. Milkovich, C.T. Herakovich, and G.F. Sykes. Space radiation effects on graphite-epoxy composite materials. Technical report, NASA Report TM 85478, 1984.
21. S.P Rawal, M.S. Misra, and R.G. Wendt. Composite materials for space applications. Technical Report N96-187472, NASA, 1990.
22. G. Yaniv, I.M. Daniel, S. Cokeing, and G.M. Martinez. Temperature effects on high strain rate properties of graphite/epoxy composites. Technical Report NASA-CR-189082, NASA, 1991.
23. Ever J. Barbero. *Introduction to Composite Materials Design.* CRC Press, 3rd edition, 2018.
24. R. Luciano and E.J. Barbero. Formulas for the stiffness of composites with periodic microstructure. *International Journal of Solids and Structures*, 31(21):2933 – 44, 1994.
25. E.J. Barbero and R. Luciano. Micromechanical formulas for the relaxation tensor of linear viscoelastic composites with transversely isotropic fibers. *International*

Journal of Solids and Structures, 32(13):1859 – 72, 1995/07/.

26. R. Luciano and E.J. Barbero. Analytical expressions for the relaxation moduli of linear viscoelastic composites with periodic microstructure. *Transactions of the ASME. Journal of Applied Mechanics*, 62(3):786 – 93, 1995.
27. *Computer Aided Design Environment for Composites (CADEC)*. http://en.cadec-online.com.
28. John W. Weeton, Dean M. Peters, and Karyn L. Thomas. *Engineers' Guide to Composite Materials*. American Society for Metals, 1987.
29. J.R. Strife and K.M. Prewo. Thermal expansion behavior of unidirectional and bidirectional kevlar/epoxy composites. *Journal of Composite Materials*, 13:264–277, October, 1979.
30. V.M. Levin. Thermal expansion coefficients of heterogeneous materials. *Mechancis of Solids*, 2:58–61, 1967.
31. V.M. Levin. Determining the elasticity and thermoelasticity constants of composite materials. *Izvestiya Akademii Nauk SSSR, Mekhanika Tverdogo Tela*, (6):137 – 45, 1976.
32. B.W. Rosen and Z. Hashin. Effective thermal expansion coefficients and specific heats of composite materials. *International Journal of Engineering Science*, 8:157–173, 1984.
33. D.E. Bowles and S.S. Tompkins. Prediction of coefficients of thermal expansion for unidirectional composites. *Journal of Composite Materials*, 23(4):370 – 88, 1989.
34. S.K. Shao-Yun Fu. *Polymers at Cryogenic Temperatures*. Springer, first edition edition, 2013.
35. I. Perepechko. *Low-Temperature Properties of Polymers*. Elsevier Science and Technology, first edition edition, 1980.
36. G. Hartwig. *Polymer Properties at Room and Cryogenic Temperatures*. Springer US, first edition edition, 1994.
37. Piyush K. Dutta. Behavior of materials at cold regions temperatures. Cold regions research and engineering laboratory, US Army Corps of Engineers, 1988.
38. J. B. Titus. Effect of low temperature (0 to -65 f) on the properties of plastic. Technical report, Plastics Technical Evolution Center, 1967.
39. M.M. Pavlick, W.S. Johnson, Brian Jensen, and Erik Weiser. Evaluation of mechanical properties of advanced polymers for composite cryotank applications. *Composites: Part A*, 2009.
40. G. Hartwig. Fibre-epoxy composites at low temperature. *Cryogenics*, 24(11):639–647, 1984.
41. Saburo Usami, H. Ejima, T. Suzuki, and K. Asano. Cryogenic small-flaw strength and creep deformation of epoxy resins. *Cryogenics*, 39:729–738, 1999.
42. B. Kneifel. *Nonmetallic Materials and Composites at Low Temperatures.*, volume Fracture properties of Epoxi resins at low temperatures. Springer, 1979.
43. V.B. Gupta, L.T. Drzal, and C. Lee. The temperature dependence of some mechanical properties of a cured epoxy resin suystem. *Polymer engineering and science*, 25(13):812–823, 1985.
44. Zhao Bo, Li Jing-wei, Li-Shu-guang, Lu Yi-hui, and Hao Ju-tao. Relationship between fracture toughness and temperature in epoxy coatings. *Polimery*,

60(4):258–263, 2015.

45. M.B. Kase. Mechanical and thermal properties of filamentary-reinforced structural composites at cryogenic temperatures. *Cryogenics*, 15:327–249, 1975.
46. A. Forghani, M. Shahbazi, N. Zobeiry, A. Poursartipand, and R. Vaziri. An overview of continuum damage models used to simulate intralaminar failure mechanisms in advanced composite materials. *Numerical Modelling of Failure in Advanced Composite Materials*, pages 151 – 173, 2015.
47. Adi Adumitroaie and Ever J. Barbero. Intralaminar damage model for laminates subjected to membrane and flexural deformations. *Mechanics of Advanced Materials and Structures*, 22(9):705 – 716, 2015.
48. E. J. Barbero and D. H. Cortes. A mechanistic model for transverse damage initiation, evolution, and stiffness reduction in laminated composites. *Composites Part B*, 41:124–132, 2010.
49. Ever J. Barbero and Javier Cabrera Barbero. Analytical solution for bending of laminated composites with matrix cracks. *Composite Structures*, 135:140 – 155, 2016.
50. Ever J. Barbero. *Finite Element Analysis of Composite Materials Using Abaqus*. CRC Press, first edition, 2013.
51. Ever J. Barbero. *Finite Element Analysis of Composite Materials Using ANSYS*. CRC Press, second edition, 2014.
52. M. M. Moure, S. Sanchez-Saez, E. Barbero, and E. J. Barbero. Analysis of damage localization in composite laminates using a discrete damage model. *Composites Part B*, 66:224–232, 2014.
53. E. J. Barbero, F. A. Cosso, R. Roman, and T. L. Weadon. Determination of material parameters for Abaqus progressive damage analysis of E-Glass Epoxy laminates. *Composites Part B:Engineering*, 46:211–220, 2013.
54. E. J. Barbero and F. A. Cosso. Determination of material parameters for discrete damage mechanics analysis of Carbon-Epoxy laminates. *Composites Part B*, 56:638–646, 2014.
55. E.J. Barbero, G. Sgambitterra, A. Adumitroaie, and X. Martinez. A discrete constitutive model for transverse and shear damage of symmetric laminates with arbitrary stacking sequence. *Composite Structures*, 93(2):1021 – 1030, 2011.
56. G. Sgambitterra, A. Adumitroaie, E.J. Barbero, and A. Tessler. A robust three-node shell element for laminated composites with matrix damage. *Composites Part B: Engineering*, 42(1):41 – 50, 2011.
57. E. J. Barbero and F. A. Cosso. Benchmark solution for degradation of elastic properties due to transverse matrix cracking in laminated composites. *Composite Structures*, 98:242–252, 2013.
58. E. J. Barbero, F. A. Cosso, and X. Martinez. Identification of fracture toughness for discrete damage mechanics analysis of glass-epoxy laminates. *Applied Composite Materials*, November:1–18, 2013.
59. Ever J. Barbero, Javier Cabrera Barbero, and Carlos Navarro Ugena. Analytical solution for plane stress/strain deformation of laminates with matrix cracks. *Composite Structures*, 132:621 – 632, 2015.
60. Mohammadhossein Ghayour, H Hosseini-Toudeshky, Meisam Jalalvand, and Ever J Barbero. Micro/macro approach for prediction of matrix cracking

evolution in laminated composites. *Journal of Composite Materials*, 50(19):2647–2659, 2016.
61. E.J. Barbero and M. Shahbazi. Determination of critical energy release rates for discrete damage mechanics analysis in ANSYS. *Theoretical and Applied Fracture Mechanics*, 92:99 – 112, 2017.
62. M.M. Moure, F. Otero, S.K. Garcia-Castillo, S. Sanchez-Saez, E. Barbero, and E.J. Barbero. Damage evolution in open-hole laminated composite plates subjected to in-plane loads. *Composite Structures*, 133:1048 – 1057, 2015.
63. M.M. Moure, S.K. Garcia-Castillo, S. Sanchez-Saez, E. Barbero, and E.J. Barbero. Influence of ply cluster thickness and location on matrix cracking evolution in open-hole composite laminates. *Composites Part B: Engineering*, 95:40 – 47, 2016.
64. M.M. Moure, S.K. Garcia-Castillo, S. Sanchez-Saez, E. Barbero, and E.J. Barbero. Matrix cracking evolution in open-hole laminates subjected to thermo-mechanical loads. *Composite Structures*, 183(-):510–520, 2018.
65. E.J. Barbero and M. Shahbazi. Determination of material properties for ANSYS progressive damage analysis of laminated composites. *Composite Structures*, 176:768–779, 2017.
66. E. J. Barbero and J. Cabrera Barbero. Determination of material properties for progressive damage analysis of carbon/epoxy laminates. *Mechanics of Advanced Materials and Structures*, 0(0):1–10, 2018.
67. Amoco. Thornel carbon fiber data sheets, 1987.
68. Cytec. Thornel carbon fiber data sheets, 2012.
69. Hexcel. Hercules carbon fiber data sheets, 1984.
70. D.S. Adams, D.E. Bowles, and C.T. Herakovich. Characteristics of thermally-induced transverse cracks in graphite epoxy composite laminates. Technical Report NASA-TM-85429, NASA, 1983.
71. S. S. Tompkins and J. G. Funk. Effects of changes in composite lamina properties on laminate coefficient of thermal expansion. *International SAMPE Electronics Conference*, 24:867 – 878, 1992. Composite lamina properties;Laminate coefficient of thermal expansion (CTE);Near zero thermal expansion;.
72. S.S. Tompkins and J.G. Funk. Sensitivity of the coefficient of thermal expansion of selected graphite reinforced composite laminates to lamina thermoelastic properties. *S.A.M.P.E. quarterly*, 23(3):55 – 61, 1992. Graphite Fiber Reinforced Composites;Lamina Thermoelasticity;.
73. MathWorks. Matlab tolerances and stopping criteria. *http://docs.scipy.org/doc/scipy-0.17.0/reference/generated/scipy.optimize.fmin.html*.
74. A.S. Crasto and R.Y. Kim. On the determination of residual stresses in fiber-reinforced thermoset composites. *Journal of Reinforced Plastics and Composites*, 12(5):545–558, 1993.
75. Chin-T. Sun and K.J. Yoon. Mechanical properties of graphite/epoxy composites at various temperatures. Technical Report HTMIAC 9, US DoD, 1988.
76. Jasson R. Maddocks. Microcracking in composite laminates under thermal and mechanical loading. Technical Report N96-16101, NASA, 1995.

77. MIL17. *Composite Materials Handbook*. Department of Defense, Volume 2 of 5, 2002.
78. J.M. Augl. Prediction and verification of moisture effects on carbon fiber-epoxy composites. Technical report, DTIC ADA079557, 1979.
79. J.M. Augl. Moisture effects on the mechanical properties of hercules 3501-6 epoxy resin. Technical report, DTIC ADA078616, 1979.
80. J.F. Derek, C.T. Herakovich, and G.F. Sykes. Space enviromental effects on graphite-epoxy composite properties and epoxy tensile properties. Technical report, NASA Report TM 89297, 1987.
81. T. L. Brown. *The effect of long-term thermal cycling on the microcracking behavior and dimensional stability of composite materials*. PhD thesis, Virginia Polytechnic Institute and State University, 1997.
82. H.L McManus. Prediction of thermal cycling induced cracking in polymer matrix composites. Technical Report NAG-1-1493.
83. H.L McManus. Prediction of thermal cycling induced matrix cracking. *Journal of Reinforced Plastics and Composites*, 15:124–140, 1996.
84. MatWeb. Material property data. *http://www.matweb.com/search/DataSheet.aspx*, 2013.
85. S.W. Tsai. *Composite Design*. Think Composites, third edition, 1987.
86. S. Kawabata. Measurement of the transverse mechanical properties of high-performance fibres. *Journal of the Textile Institute*, 81(4):432–447, 1990.
87. B.J. Knouff, S.S. Tompkins, and N. Jayaraman. The effect of graphite fiber properties on microcracking due to thermal cycling of epoxy-cyanate matrix laminates. *Composite Materials: Fatigue and Fracture, ASTM STP 1230*, 5:268–282, 1994.
88. D. Belitskus. *Fiber and Whisker Reinforced Ceramics for Structural Applications*. CRC Press, 1993.
89. Y Huang and RJ Young. Effect of fibre microstructure upon the modulus of pan-and pitch-based carbon fibres. *Carbon*, 33(2):97–107, 1995.
90. L.A. Pilato and M.J. Michno. *Advanced Composite Materials*. Springer Science and Business Media, 1994.
91. N.P. Bansal and J. Lamon. *Ceramic Matrix Composites: Materials, Modeling and Technology*. John Wiley and Sons, 2014.
92. P. Arsenovic. Nonlinear elastic characterization of carbon fibers. *Fiber, Matrix, and Interface Properties, ASTM.*, pages 2–8, 1996.
93. B. Christopher and J. Zakrzewski. Moisture absorption and mechanical properties for high modulus pitch 75 graphite fiber/modified cyanate ester resin laminates. *Journal of Design and Optical Instruments*, 1690, 1992.
94. J. F. Helmer and R. J. Diefendorf. Transverse thermal expansion of carbon fiber/epoxy matrix composites. In *Proceedings of 5th International Symposium on Composite Metallic Materials*, pages 15–20, 1983.
95. K. Y. Donaldson and D. P. H. Hasselman H. D. Bhatt. Role of interfacial gaseous heat transfer and percolation in the effective thermal conductivity of two uniaxial carbon-fiber-reinforced glass matrix composites. In *Proceedings of 17th Annual Conference on Composites and Advanced Ceramic Materials*, pages 335–340, 1993.

96. D.F. Adams. Laminate analyses, micromechanical creep response, and fatigue behavior of polymer matrix composite materials. Technical Report UWME-DR-201-108-1, University of Wyomin, Laramie, WY, 1982.
97. SIMULIA. *Abaqus Documentation. Analysis Users Guide. 21.1.2 Material data definition.* SIMULIA, 6.13 edition.
98. E. Orowan. Energy criteria of fracture. Technical Report N5ori-07870, MIT, Cambridge, MA, 1954.
99. G. R. Irwin. Analysis of stresses and strains near the end of a crack traversing a plate. *Journal of applied mechanics*, 24(3):361–364, 1957.
100. C.G. Davila, C.A. Rose, and E.V. Iarve. *Mathematical Methods and Models in Composites*, volume 5, chapter Modeling fracture and complex crack networks in laminated composites, pages 297 – 347. World Scientific, 2014.
101. E Adolfsson and P Gudmundson. Matrix crack initiation and progression in composite laminates subjected to bending and extension. *International Journal of Solids and Structures*, 36(21):3131–3169, 1999.
102. J. Nairn and S. Hu. Matrix microcracking. In R. Talreja, editor, *Damage Mechanics of Composites Materials*, pages 187–243. Elsevier, 2004.
103. E. Tschegg, K. Humer, and H. W. Weber. Mechanical properties and fracture behaviour of polyimide (sintimid) at cryogenic temperatures. *Cryogenics*, 31(10):878–883, 1991.
104. K. Humer, E. K. Tschegg, and H.W. Weber. Tensile, fracture and thermal properties of polyarylates at room and cryogenic temperatures. *Cryogenics*, 33(7):686–691, 1993.
105. A. J. Kinlonch. *Fracture Behaviour of polymers*. Applied Sciences Publishers, 1983.
106. U. Saburo, H. Ejima, T. Suzuki, and K. Asano. Cryogenic small-flaw strength and creep deformation of epoxy resins. *Cryogenics*, 39:729–738, 1999.
107. F. Sawa. Evaluation of fracture toughness of epoxy resin for cryogenic use. *Journal of Cryogenics and Superconductivity Society of Japan*, 30:129–134, 1999.
108. G. Hartwig. Fracture properties of polymers and composites at cryogenic temperatures. *Advances in cryogenic engineering*, 1986.
109. G. Hartwig. Low-temperature properties of resins and their correlations. *Advances in cryogenic engineering*, 22:283–290, 1977.
110. L.E. Evseeva and S.A. Tanaeva. Thermophysical properties of epoxy composite materials at low temperatures. *Cryogenics*, 35:277–279, 1995.
111. E.J. Barbero and J. Cabrera Barbero. Determination of material properties for progressive damage analysis of carbon/epoxy laminates. *Mechanics of Advanced Materials and Structures*, 2018. http://dx.doi.org/10.1080/15376494.2018.1430281.
112. Python. Xlsxwriter module documentation. *https://pypi.python.org/pypi/XlsxWriter*.